UC Santa Barbara

UC Santa Barbara Electronic Theses and Dissertations

Title

Algorithms and Protocols for Wideband Distributed Beamforming

Permalink

https://escholarship.org/uc/item/9wx4q7br

Author

Gencel, Muhammed Faruk

Publication Date

2018

Peer reviewed|Thesis/dissertation

eScholarship.org Powered by the California Digital Library
University of California

University of California
Santa Barbara

Algorithms and Protocols for Wideband Distributed Beamforming

A dissertation submitted in partial satisfaction
of the requirements for the degree

Doctor of Philosophy
in
Electrical and Computer Engineering

by

Muhammed Faruk Gencel

Committee in charge:

Professor Upamanyu Madhow, Chair
Professor Heather Zheng
Professor Kenneth Rose
Professor João P. Hespanha

June 2018

The Dissertation of Muhammed Faruk Gencel is approved.

Professor Heather Zheng

Professor Kenneth Rose

Professor João P. Hespanha

Professor Upamanyu Madhow, Committee Chair

June 2018

Algorithms and Protocols for Wideband Distributed Beamforming

Copyright © 2018

by

Muhammed Faruk Gencel

To my dear family, with love and gratitude

Curriculum Vitæ

Muhammed Faruk Gencel

Education

2018	Ph.D. in Electrical and Computer Engineering, University of California, Santa Barbara.
2014	M.S. in Electrical and Computer Engineering, University of California, Santa Barbara.
2013	Bachelor of Science, Electrical and Electronics Engineering, Bilkent University, Ankara, Turkey.

Publications

1. **M. F. Gencel**, M. E. Rasekh, and U. Madhow, "Scaling wideband distributed transmit beamforming via aggregate feedback," *in Communications (ICC), 2015 IEEE International Conference on.* IEEE, 2015, pp. 2356-2362.
2. **M. F. Gencel**, M. E. Rasekh, and U. Madhow, "Distributed transmit beamforming with one bit feedback revisited: How noise limits scaling," *in Information Theory (ISIT), 2015 IEEE International Symposium on.* IEEE, 2015, pp. 2041-2045.
3. **M. F. Gencel**, M. E. Rasekh, and U. Madhow, "Noise-resilient scaling for wideband distributed beamforming," *in Signals, Systems and Computers, 2015 49th Asilomar Conference on.* IEEE, 2015, pp. 276-280.
4. **M. F. Gencel**, U. Madhow and J. Hespanha, "RF Source Seeking using Frequency Measurements," *in Proc. Int. Workshop IEEE Signal Process. Adv. Wireless Commun.*, Greece, Jun. 2018.
5. **M. F. Gencel**, M. E. Rasekh and U. Madhow, "Distributed Base Station: A Concept System for Long-Range Broadband Wireless Access." *arXiv preprint arXiv: 1803.02877* (2018).

Abstract

Algorithms and Protocols for Wideband Distributed Beamforming

by

Muhammed Faruk Gencel

The potential performance gains from distributed Multiple-Input Multiple-Output (MIMO) have been established by theory, simulations and experimental demonstrations over the past decade. By synchronizing their signals in frequency and phase at the receiver, multiple cooperating transmitters achieve an N-fold increase in received power compared to noncoherent signal combination, or power pooling, and an N^2-fold increase in received power compared to that for a single transmitter. The first part of this thesis investigates algorithms for Distributed MIMO (DMIMO). A well-known one-bit feedback scheme is extended to wideband systems by introducing additional feedback bit to enforce phase continuity across OFDM subcarriers to utilize available system bandwidth. It is also shown, however, that low signal to noise ratio (SNR) is a fundamental limitation for the well-known one-bit feedback algorithm and its variants. This limitation motivates the development of explicit training strategies that can operate at low SNR while keeping the number of feedback bits low. Explicit training strategies are extended to wideband setting by simple interpolation over OFDM subcarriers and sparse time domain modeling of outdoor channels.

The second part of this thesis presents two concept systems that could be based around the DMIMO paradigm: distributed base station and distributed 911. The use of a distributed base station enables distributed transmit beamforming at large carrier wavelengths to achieve significant range extension and increased downlink data rate, providing a low-cost infrastructure for applications such as rural broadband. The proposed

cross-layer design of distributed base station is based on explicit training with heavily quantized feedback. The feasibility of such a system is explored using outage capacity analysis for both the downlink and the feedback link. System performance is quantified in different channel conditions. The distributed 911 concept system enables multiple nodes to communicate with a distant search-and-rescue vehicle which tries to approach to the nodes by using radio frequency trail of the periodic beacons transmitted by the nodes. As an initial step to realize this, an algorithm using Doppler frequency measurements is devised for a quasi-stationary radio frequency emitting source sought by an unmanned aerial vehicle (UAV). Our algorithm uses periodic beacons from the emitter to continuously adapt its trajectory by using consecutive frequency measurements and provides a great improvement over prior received signal strength based source seeking algorithms.

This thesis includes the following publications:

- ©2015 IEEE. Reprinted, with permission, from M.F Gencel, M.E Rasekh and U. Madhow. Scaling wideband distributed transmit beamforming via aggregate feedback. *In IEEE International Conference on Communications (ICC),* June 2015

- ©2015 IEEE. Reprinted, with permission, from M.F Gencel, M.E Rasekh and U. Madhow. Distributed transmit beamforming with one bit feedback revisited: How noise limits scaling. *In IEEE International Symposium on Information Theory (ISIT),* June 2015

- ©2015 IEEE. Reprinted, with permission, from M.F Gencel, M.E Rasekh and U. Madhow. Noise-resilient scaling for wideband distributed beamforming. *In 49th Asilomar Conference on in Signals, Systems and Computers,*, November 2015

- ©2018 IEEE. Reprinted, with permission, from M.F Gencel, U. Madhow and J. Hespanha. RF Source Seeking using Frequency Measurements. *In Proc. Int. Workshop IEEE Signal Process. Adv. Wireless Commun.,* June 2018

Contents

Curriculum Vitae **v**

Abstract **vi**

List of Figures **xi**

List of Tables **xiii**

1 Introduction **1**
- 1.1 Background . . . 3
- 1.2 Algorithms for Feedback-Based Distributed Beamforming . . . 4
- 1.3 Concept System: Distributed Base Station . . . 6
- 1.4 Concept System: Distributed 911 . . . 7
- 1.5 Organization of the Thesis . . . 8

2 Wideband Distributed Beamforming Based on Aggregate Feedback **9**
- 2.1 Description of One Bit Feedback Algorithm . . . 10
- 2.2 System Model in Frequency Selective Channels . . . 11
- 2.3 Extension to Wideband Systems Using 2 bit-feedback Algorithm . . . 15
- 2.4 Performance Analysis . . . 17

3 Analysis of One Bit Feedback Algorithm in the Presence of Noise **22**
- 3.1 One bit feedback algorithm with memory . . . 23
- 3.2 Analysis of One Step Progression of Received Signal Strength . . . 24
- 3.3 Performance Analysis with Received Signal Strength Memory . . . 27
- 3.4 Numerical Results . . . 30

4 Distributed Base Station **34**
- 4.1 Introduction . . . 34
  - 4.1.1 Related Work . . . 36
- 4.2 System and Channel Model . . . 37
  - 4.2.1 DBS system model . . . 37

4.2.2 Signal Model . . . 37
4.2.3 Channel Model . . . 38
4.3 Narrowband Feedback-based Distributed Beamforming Techniques . . . 39
4.3.1 Deterministic Orthogonal Sequence Training . . . 40
4.3.2 Alternative Strategies . . . 44
4.3.2.1 Successive Deterministic Distributed Beamforming . . . 44
4.3.2.2 Randomized two bit feedback algorithm (R2BF) . . . 45
4.3.2.3 Modified two bit feedback algorithm (M2BF) . . . 46
4.3.3 Numerical results and comparisons . . . 46
4.4 Extension to Wideband using OFDM . . . 50
4.4.1 Using simple interpolation . . . 50
4.4.2 Using time-domain sparsity . . . 53
4.4.3 Simulation results . . . 54
4.5 System Performance . . . 56
4.5.1 Downlink Performance . . . 58
4.5.2 Feedback link . . . 62

5 Distributed 911: RF Source Seeking as a Building Block 67
5.1 Introduction . . . 67
5.2 Channel Model . . . 70
5.3 The Algorithm for Source Seeking . . . 72
5.3.1 Trajectory adaptation . . . 74
5.4 Analysis . . . 76
5.5 Simulation Results . . . 77

6 Conclusion and Future Work 81
6.1 Algorithms and Protocols . . . 81
6.2 Concept Systems . . . 82

Bibliography 84

List of Figures

1.1 System model for distributed beamforming 6

2.1 N transmitters beamforming over frequency selective channels, using feedback broadcast from the receiver 12
2.2 Frequency response of realization of a wideband channel with $\tau_d = 4.7\mu s$, over $N = 1024$ subcarriers, with a total bandwidth of $W = 10$ MHz and $f_c = 2.5$ GHz 13
2.3 Amplitude and phase of net channel response of 10 transmitter for A) non-coherent combinations, B) coherent combination after convergence of 1-bit feedback, C) coherent combination and smoothing with 2-bit feedback . 18
2.4 Convergence of 2-bit feedback with time 20
2.5 MSE of interpolation of channel estimate from subset of subcarriers . . . 21

3.1 Effect of random phase perturbations on the total received signal 25
3.2 Markov chain 28
3.3 2D histogram of noiseless versus noisy RSS increments ($N = 100$ transmitters and window size $M = 4$) compared against the analytical joint Gaussian distribution. 31
3.4 Theoretical values of RSS drifts with window size $M = 4$ and for $N = 100$ transmitters in different noise levels 32
3.5 Simulated normalized RSS values vs SNR for different number of transmitters, RSS memory size $M = 4$ and random phase rotations $\delta_i \sim \mathcal{U}(-\Delta, \Delta)$ 33

4.1 The Distributed Base Station Concept System. 35
4.2 Evolution of the distributed beamforming approaches in a noiseless setting for $N = 100$ nodes 48
4.3 Evolution of the distributed beamforming approaches for $N = 100$ nodes at SNR per node -5 dB 49
4.4 Normalized beamforming gains for SDDB and DOST for different number of feedback bits 50
4.5 Proposed comb type pilot arrangement for channel estimation over OFDM grid 51

4.6 Standard 2D-grid type pilot placement is not well matched to a DBS OFDM downlink. 53
4.7 A realization of time domain channel estimation algorithm using subset of subcarriers (32 out of 256) and reconstructed phase of the channel by time domain estimates 55
4.8 RSS averaged over OFDM subcarriers vs SNR per node for $N = 10$ nodes 56
4.9 DBS frame structure with a slow feedback link. 57
4.10 Ergodic capacity and 1% outage rates (b/s/Hz) versus number of nodes for narrowband flat fading channel at SNR $= -5$ dB 62
4.11 1% outage rates (b/s/Hz) vs N for wideband channel at average SNR $= -5$ dB 63
4.12 1% outage rates vs per node SNR for wideband channels using 10% of the 20 MHz uplink bandwidth with single node, best node and ideal receive beamforming with using $N = 10$ nodes 65

5.1 System model in 2D, scatterers on a disk around the source 70
5.2 Initial circular motion of the UAV 75
5.3 Updating the direction of the UAV by perturbing the direction with $\pm\delta_k$ 76
5.4 An example trajectory with the 0 dB average SNR with the initial distance of 5 km 79
5.5 Frequency measurements and the received signal strength trough the route in Figure 5.4 79
5.6 Histogram of the total distance traveled to get the 200m vicinity of the source (mean ~ 5.5km) 80
5.7 Histogram of the total distance traveled to get the 200m vicinity of the source using random initialization, without using stage 1 (mean ~ 6km) 80

List of Tables

4.1 EPA channel model 40
4.2 Link Level System parameters 52

5.1 Simulation parameters 78

Chapter 1

Introduction

Over the past decade, Distributed Multiple Input Multiple Output (DMIMO) systems have received significant attention due to their potential for energy-efficient wireless communications. Distributed transmit beamforming is a subclass of DMIMO and refers to a class of communication schemes in which a group of nodes cooperate to deliver a common message to an intended receiver. A cluster of N cooperating transmitter nodes emulates a virtual antenna array that forms a beam towards a desired receiver. Ideally, this provides an N-fold increase in the received signal to noise ratio (SNR) due to an increase in transmit power and an additional N-fold beamforming gain in case of coherent phase synchronization resulting in an N^2-fold gain in SNR compared to that for a single transmitter. The goal in distributed beamforming is to leverage this N^2 power gain in extending the communication range, increasing the data rate, or increasing power efficiency. The fundamental bottleneck is the timing, frequency, and phase synchronization of the independent nodes whose signals originate from independent local oscillators. Unlike classical phased-array antennas, a distributed antenna array has an unknown geometry, which causes an additional phase offset.

The focus of this thesis is to design and analyze algorithms and protocols that uti-

lize the available bandwidth in wideband distributed transmit beamforming and achieve phase synchronization through limited explicit feedback. We limit attention to systems with aggregate feedback, in which the receiver broadcasts feedback that is not directed at any particular transmitter node. This allows for protocol-level scalability in the number of transmitter nodes. The key contributions of this thesis are listed as follows. First, we extend the well-known one bit feedback algorithm to wideband. Second, we show that the one bit feedback algorithm and its variants are fundamentally limited by noise. Thus, a near-ideal beamforming gain cannot be obtained by these algorithms. Third, we propose a distributed orthogonal sequence training (DOST) algorithm that overcomes receiver noise by suitably averaging over time. We extend this algorithm to wideband scenarios via a simple interpolation over Orthogonal Frequency Division Multiplexing (OFDM) subcarriers. Based on the DOST algorithm, we investigate cross layer design and analysis of a concept system termed distributed base station (DBS), which aims to increase downlink range and/or spectral efficiency. We analyze the potential gains of a DBS via outage capacity analysis. We observe that the feedback channel may become a bottleneck unless sophisticated distributed reception strategies are employed. Fourth, we propose a trajectory planning algorithm for an unmanned aerial vehicle (UAV) as an initial step to realize a concept system that we term distributed 911. An emitter broadcasts a periodic pilot signal from an unknown location which helps an emergency vehicle determine its trajectory using frequency measurements and subsequently approach the emitter. We show that the algorithm enables the UAV to head towards the unknown emitter location.

1.1 Background

Realization of distributed MIMO requires tight synchronization among the virtual antenna array nodes to achieve constructive interference at the receiver. The key to achieve distributed beamforming which requires tight synchronization is the use of feedback from the receiver using either closed loop synchronization via aggregate explicit feedback or open loop synchronization which makes use of channel reciprocity [1, 2].

A direct approach for distributed beamforming in frequency division duplex (FDD) systems is to estimate forward link channels at the target node and send quantized estimates of the channels to each transmit antenna explicitly. This approach works when there is a limited number of antennas, but the feedback overhead and the coordination requirement across nodes become excessive as the number of antennas increases. Aggregate feedback in which the receiver is not directed to any specific node can be used to achieve scalability in the number of antennas.

The one bit feedback algorithm is the first to use aggregate feedback to achieve distributed beamforming [3]. This algorithm iteratively perturbs the phase of the each signal randomly and employs one bit of feedback per iteration from the receiver to align the phases of each signal. It is provably convergent to an ideal beamforming solution in an ideal setting [4, 5]. This simple and scalable approach has formed the basis of several prototypes for all-wireless distributed beamforming [6, 7, 8, 9, 10]. The one bit feedback algorithm is further improved in terms of convergence time by exploiting the knowledge from the previous iterations [11] and using an additional feedback bit per iteration [12]. In [13], the authors propose a variable perturbation size to decrease the convergence time, which improves robustness in time-varying channels. The one bit feedback algorithm was also extended to wideband dispersive channels by using an additional bit to enforce phase continuity across frequency [14] with simple interpolation. The performance of the

original one bit feedback algorithm has been shown to be degraded receiver noise in [15]. A noise resilient training-based distributed beamforming approach was presented in [16] and extended to wideband systems by exploiting time domain sparsity of the outdoor environments.

While the focus of this thesis is explicit feedback based systems when channel reciprocity is not available, it is worth mentioning the reciprocity based time division duplexed (TDD) systems, in which downlink and uplink channels operate in the same frequency band. Reciprocity based protocols for distributed beamforming were proposed in [17, 18] in which channels from a virtual antenna array are estimated from the signal emitted from the target node. The non-reciprocal transceiver chain in these links was addressed in [19] for wideband transmit beamforming. Emulation of the virtual antenna array by pre-synchronized cooperating nodes were experimentally demonstrated in [20, 21]. Reciprocity based operational 802.11 distributed MIMO system was demonstrated in [22].

Distributed beamforming systems that rely on a fast wired backhaul among infrastructure nodes with WiFi access points [23] and cellular base stations [24, 25, 26] were studied. However, the emphasis of this thesis is to design all-wireless distributed beamforming systems that achieve the potential gains from massive MIMO [27, 28, 29] without relying on a fast wired backhaul.

1.2 Algorithms for Feedback-Based Distributed Beamforming

A well-known approach to distributed transmit beamforming with explicit aggregate feedback is stochastic ascent, in which the transmitters use small random phase pertur-

bations while the receiver provides a single feedback bit per iteration [3]. For wideband OFDM systems, application of the one bit feedback algorithm separately to each subcarrier results in phase discontinuities in the net received signal across frequency. Phase continuity is necessary for standard OFDM channel estimation algorithms at the receiver. We propose a second feedback bit to the one bit feedback algorithm to ensure phase continuity [14].

Distributed beamforming algorithms are particularly interesting in low-SNR scenarios where a single node cannot maintain a reliable high-rate link. We show that noise is a fundamental limitation for the one bit feedback algorithm when the SNR per node is small [15]. The implication of the noise barrier is that we cannot arbitrarily extend the communication range by scaling the number of nodes using the one bit feedback algorithm and its variants.

System Model

We consider a simple narrowband system model to illustrate feedback based distributed beamforming algorithms. As depicted in Figure 1.1, N transmitters send a common message to a receiver over a noisy, flat fading channel, with feedback from the receiver used by the transmitters to adjust their phases so as to align at the receiver. Frequency synchronization can be achieved by each node synchronizing to the receiver node (as in prototypes such as [8]) or to a master node within the virtual antenna array [9], and the effect of small residual frequency offsets can be included within the noise term. We assume that the nodes in the virtual antenna array are synchronized in timing and frequency. We focus on the phase synchronization which requires channel state information at the transmitter (CSIT). Ignoring the common message, the received baseband

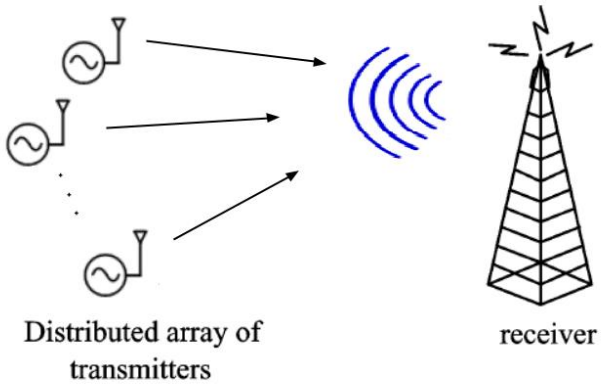

Figure 1.1: System model for distributed beamforming

sample is given by

$$Z = \sum_{i=1}^{N} a_i e^{j(\theta_i+\gamma_i+\psi_i)} + \bar{w}, \tag{1.1}$$

where a channel seen by transmitter i is the complex gain $h_i = a_i e^{\psi_i}$, γ_i is the receiver's phase offset relative to transmitter i, θ_i is the adjustable phase for transmitter i, and $\bar{w} \sim CN(0, N_0)$ is the receiver noise. The received signal strength (RSS) is given by $Y = |Z|$. The ideal beamforming solution corresponds to $\theta_i = -(\gamma_i + \psi_i)$ (modulo any constant phase offset independent of i), and yields the maximum possible value of noiseless RSS as $Y_{max} = \sum_{i=1}^{N} a_i$. Additionally, we use normalized RSS as the performance metric which is RSS divided by the number of virtual antenna nodes $y = \frac{Y}{N}$.

1.3 Concept System: Distributed Base Station

The DBS concept system comprises N low-cost nodes without wired connections among them. Our goal is to leverage N^2-fold SNR gain at the receiver provided by

distributed beamforming to increase downlink range and/or spectral efficiency. While DBS can be used in existing WiFi and LTE bands, it is particularly interesting for white space frequencies (e.g., 50-800 MHz). White space frequencies propagate well, and hence are preferred in long-range applications such as rural broadband. However, good propagation also leads to poor spatial reuse when employing omnidirectional transmission. Beamforming using multiple antennas can enhance spatial reuse, but centralized antenna arrays are bulky at large wavelengths. DBS allows the use of low-cost transmit nodes with moderate transmit power to emulate a powerful transmitter with a highly directional steerable antenna.

We propose a feedback based adaptation strategy which is robust against the low per-node SNR at increased range [16]. We extend narrowband distributed beamforming across OFDM subcarriers using a simple interpolation across a subset of designated pilot subcarriers, exploiting the continuity across frequency imposed by time domain channel sparsity. Given the extended range for the DBS concept system, feedback link and mobility of the channel could be a bottleneck. We show that significant performance gains can be achieved with standard uplink reception in relatively low mobility scenarios. We further discuss possible approaches for enhancing the feedback link when the channel varies more rapidly.

1.4 Concept System: Distributed 911

The distributed 911 (D911) concept system is based on emergency scenarios such as single or multiple mobile devices trying to reach a distant emergency vehicle for high-speed communication or to draw the vehicle to the current location.

We focus on RF source seeking as a building block to the D911 concept system. A quasi-stationary emitter broadcasts a pilot signal, and a mobile UAV tries to approach

the unknown emitter location in the shortest possible time. We propose and evaluate a trajectory planning algorithm for the UAV. Our algorithm consist of two stages. First, the UAV estimates the initial direction of the emitter by making a circular motion. Then, it continuously updates its trajectory with small perturbations on its heading direction using frequency measurements based on signals coming from the quasi-stationary emitter. We show that the proposed algorithm converges towards the emitter direction. Simulation results illustrate that the proposed algorithm significantly reduces the time required to approach the RF source when compared to prior source seeking methods.

1.5 Organization of the Thesis

The remainder of this thesis is organized as follows. Chapter 2 presents the extension of the one bit feedback algorithm (in a noiseless setting) to wideband dispersive channels, presenting an approach for imposing phase continuity across frequency. In chapter 3, we investigate the one bit feedback algorithm in a noisy scenario and show that there is a fundamental limitation in low-SNR regimes. Chapter 4 investigates the DBS concept system. Chapter 5 presents an RF source seeking algorithm for a UAV trying to approach an unknown emitter location which is a building block for a distributed 911 system. Chapter 6 presents concluding remarks, open questions, and potential future work on DBS and RF source seeking.

Chapter 2

Wideband Distributed Beamforming Based on Aggregate Feedback

We investigate distributed transmit beamforming over wideband frequency selective channels. A cluster of cooperating transmitters sends a common message, while the receiver is oblivious to the number of transmitters. A naive approach is to use well-known one bit feedback algorithm [3] over each OFDM subcarrier. This achieves beamforming gain on each subcarrier, but the effective channel seen by the receiver has severe phase discontinuities across frequency. This is incompatible with standard OFDM channel estimation techniques, which require phase smoothness across subcarriers [30]. We propose the use of a second bit feedback per subcarrier to achieve phase continuity in addition to beamforming gain acquired by the one bit feedback algorithm. The performance of the proposed algorithm is validated by simulations.

In this chapter, we first describe the one bit feedback algorithm in an ideal narrowband scenario. We demonstrate the phase discontinuities created by its application to a wideband OFDM system. We then propose an addition of a bit for phase continuity. Finally, simulation results illustrate that the proposed algorithm achieves phase smoothness

across frequency, which enables the use of classical channel estimation algorithms.

2.1 Description of One Bit Feedback Algorithm

The one bit feedback algorithm is a simple iterative procedure that synchronizes the received signals corresponding to all the transmitters without attempting to explicitly estimate channel states. The system model is illustrated in Figure 1.1 in which N nodes cooperate to send a common message. In the one bit feedback procedure, time is divided into slots and each transmitter $i \in \{1 \dots N\}$ applies a beamforming weight of $1e^{j\theta_i(k)}$ to its transmitted signal in slot k and the RSS measured at the ideal receiver is the RSS at the timeslot k is

$$Y(k) = \left| \sum_{i=1}^{N} a_i e^{j(\theta_i(k)+\gamma_i(k)+\psi_i(k))} \right|. \tag{2.1}$$

In each slot k, each transmitter applies a random perturbation if δ_i to its beamforming weight as in phase $\theta_i(k)$. At the end of the slot the receiver broadcasts one bit of feedback indicating whether or not the RSS has improved compared with the previous iteration. Upon receiving the feedback, transmitters adopt the latest beamforming phase if RSS has improved and undo the perturbations if it has degraded. This procedure is repeated until coherence is achieved. The resulting beamforming phases compensate for the phase of the channel response as well as the phase offsets of the local oscillators. The feedback from the receiver based on the received power observation in iteration n is formulated as:

$$F(k) = \begin{cases} 1 & Y(k) > Y_{max}(k) \\ 0 & Y(k) < Y_{max}(k) \end{cases}, \tag{2.2}$$

where $Y_n(k)$ is the RSS measured at the reciver in kth slot and $Y_{max}(k)$ is the maximum RSS measured so far as

$$Y_{max}(k) = \max_{0<t<k} Y(t).$$

Each transmitter updates its phase according to the feedback from receiver as follows.

$$\theta_i(k+1) = \begin{cases} \theta_i(k) & F(k) = 0 \\ \theta_i(k) + \delta_i & F(k) = 1 \end{cases}. \tag{2.3}$$

In an ideal scenario, one bit feedback algorithm is provably convergent to the optimal RSS value [5] with the proper selection of distribution to generate δ_i. While the algorithm maximizes the RSS, the received complex baseband signal ends up to a random phase as follows

$$Z = \left(\sum_{i=1}^{N} a_i \right) e^{j\zeta} \tag{2.4}$$

where ζ is uniformly distributed on the $[0, 2\pi)$.

2.2 System Model in Frequency Selective Channels

As depicted in Figure 2.1, we consider a cluster of N cooperating transmitters that wish to communicate a common message to a distant destination. The channel between the ith transmitter and the destination is denoted by $H_i(f)$, $i = 1, ..., N$. In our simulations, we model these channels as independent realizations from a bandwidth dependent tapped delay line model with exponential power delay profile [31] and all realizations are normalized to power of 0 dB. The channel impulse response is modeled as

$$h(t) = \sum_{l=1}^{k} \alpha_l \delta(t - \frac{l}{W}) \tag{2.5}$$

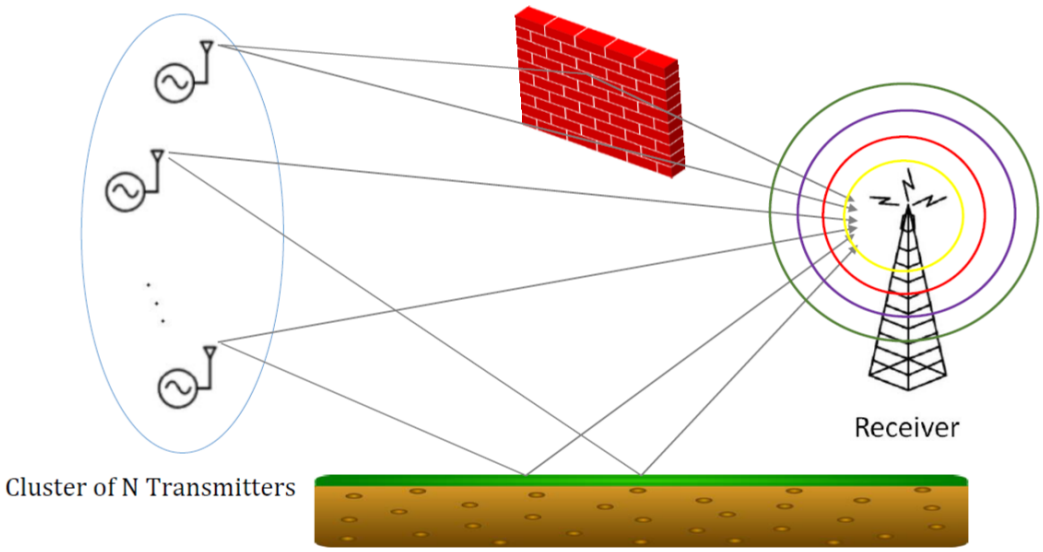

Figure 2.1: N transmitters beamforming over frequency selective channels, using feedback broadcast from the receiver

where W is the bandwith of the transmitted signal and $k = \tau_d W$ assuming there are no multipath components after the delay spread τ_d and amplitudes of the taps are

$$\alpha_l \sim CN(0, ab^l),$$

where $b = exp(-\frac{1}{W\tau_{rms}})$ and $a = 1 - b$. Figure 2.2 shows a typical channel realization with root mean squared delay $\tau_{rms} = 1\mu s$ as a typical RMS delay spread value in an urban area [32], $W = 10$ MHz, $\tau_d = 4.7\mu s$ and carrier frequency $f_c = 2.5$ GHz. We note that that there are several significant fades.

We consider OFDM with M subcarriers, with subcarrier spacing smaller than the channel coherence bandwidth. We assume that the transmitters are synchronized in terms of clock and carrier frequency (this can be achieved by a number of mechanisms, including using a master-slave architecture), but have timing and phase offsets that are *a priori* unknown. Assuming that the transmitters are coarsely synchronized in timing

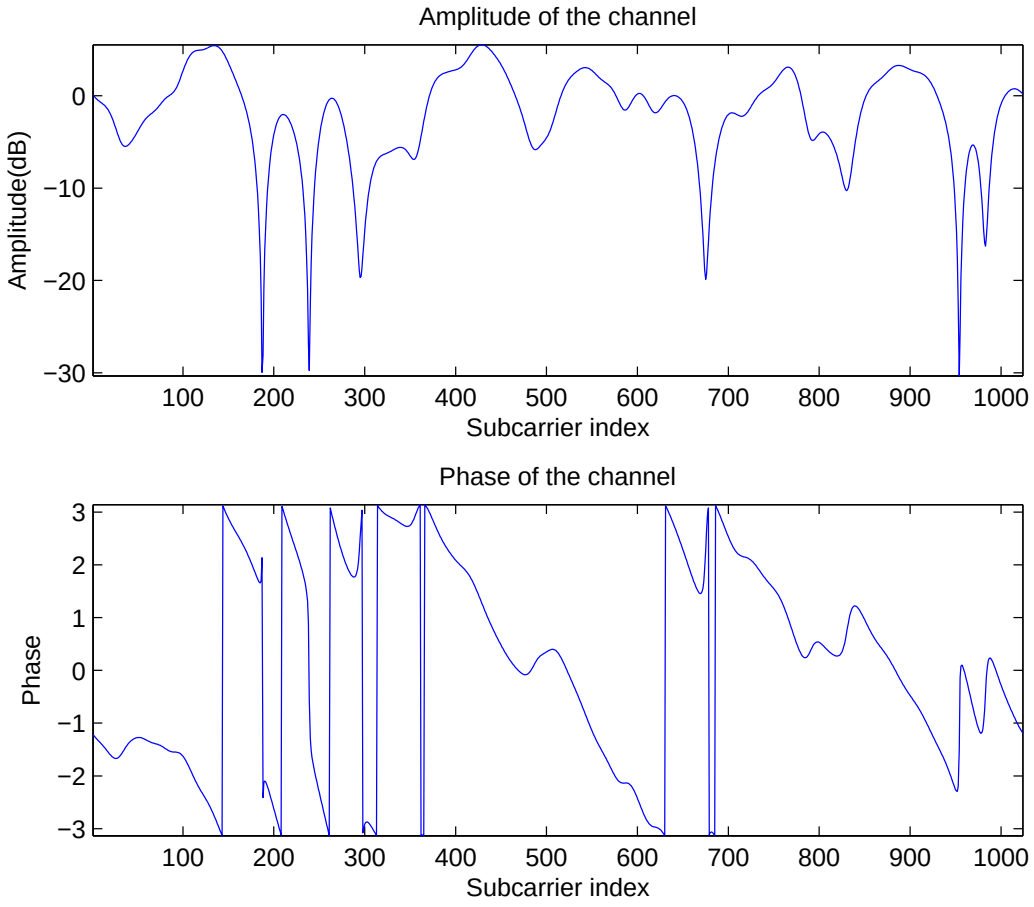

Figure 2.2: Frequency response of realization of a wideband channel with $\tau_d = 4.7\mu s$, over $N = 1024$ subcarriers, with a total bandwidth of $W = 10$ MHz and $f_c = 2.5$ GHz

such that residual offsets are significantly smaller than the channel time dispersion, we can absorb these timing offsets within the OFDM cyclic prefix. Thus, the key problem that we focus on here is the problem of coherent phase combining for each subcarrier

We are interested in regimes in which the received SNR corresponding to any given transmitter is too low to permit reliable communication at the desired rates. If the (loosely synchronized) transmitters emit a common message at an agreed upon time,

then the effective channel seen by the receiver is

$$G_{nc}(f) = \sum_{n=1}^{N} H_n(f) \tag{2.6}$$

where the subscript denotes that the channels from different transmitters are being combined noncoherently. Thus, while the net received power increases (assuming each transmitter sends at a fixed power), we still see significant frequency selective behavior, as shown in Figure 2.3(a), which shows a typical effective channel obtained from such noncoherent power pooling.

If each transmitter knows its channel to the receiver, the optimal strategy, subject to a per-transmitter power constraint, is to employ waterfilling. However, we consider a suboptimal strategy in which each transmitter simply adjusts its phase at each subcarrier to compensate for the channel, while keeping its power constant across subcarriers. Specifically, if the nth transmitter applies a precoder of the form

$$P_n(f) = e^{-j\angle H_n(f)}$$

then the net channel obtained is

$$G_c(f) = \sum_{n=1}^{N} P_n(f)H_n(f) = \sum_{n=1}^{N} |H_n(f)| \tag{2.7}$$

which is termed as the ideal beamforming solution. Figure 2.3.a benchmark plot shows a typical effective channel obtained from ideal beamforming. In addition to power pooling and beamforming gains at each frequency, we also notice a diversity gain resulting in a significant reduction in frequency selectivity.

As explained in the previous section, the one bit feedback algorithm applied indepen-

dently to each subcarrier leads to a solution of the form

$$G_{1bit}(f) = e^{j\zeta(f)} \sum_{n=1}^{N} |H_n(f)| \tag{2.8}$$

so that we are achieving beamforming gain at each frequency, but with arbitrary frequency-dependent phase shifts $\zeta(f)$ because we are not coordinating across subcarriers. Thus, the smoothness of phase across frequency that is a characteristic of natural channels, and is relied upon by receiver estimation algorithms, gets destroyed.

We show that a simple modification which runs in parallel to the one bit feedback algorithm, in which the receiver sends back 1 additional bit (per subcarrier) to help enforce phase continuity, can be used to approach the ideal beamforming solution up to a constant phase offset. This allows the receiver to use standard channel estimation algorithms that exploit smoothness of phase across frequency once it switches to decision-directed or pilot-based estimation.

2.3 Extension to Wideband Systems Using 2 bit-feedback Algorithm

A wideband frequency selective channel is parallelized into flat fading subcarriers using OFDM, hence we can directly apply the narrowband one bit algorithm. However, the beamforming phases evolve independently for different subcarriers, which results in a lack of continuity in the received signal phase across subcarriers. As shown in Figure 2.3, the noncoherent benchmark for 10 transmitters has a smooth phase response at the receiver, but the phase response after adaptation based on parallel 1-bit feedback algorithms exhibits severe discontinuities. This can be problematic when using a standard OFDM receiver, where typically a number of subcarriers are reserved as pilots for channel

estimation and no data is transmitted on them. The receiver interpolates the channel response between these pilots to obtain estimates for the channel response of all other subcarriers. These channel estimates are then used to decode the symbols sent on the data carrying subcarriers. After the initial training phase, our goal is to treat cluster of nodes as a single transmitter at the receiver side. We therefore modify the 1-bit algorithm to provide an effective channel that is smooth across subcarriers.

In order to obtain channel continuity, an additional bit of feedback is sent by the receiver for each subcarrier demanding all transmitters to either increase the phase of their beamforming weight by a predefined increment of γ or remain at the same phase for that subcarrier (on top of their individual random perturbations for the one bit algorithm). In order to achieve phase continuity at the channel seen by receiver, the receiver compares the phase of each subcarrier with the average phase of all subcarriers and send feedback that will bring this phase closer to the average. For iteration k and subcarrier frequency f_m, the feedback decision for the second bit at the receiver is formulated by defining $g[f_m, k]$ such that:

$$g[f_m, k] = Y^*[f_m, k] \sum_{j \neq k}^{M} Y[f_j, n]$$

for $m = 1, .., M$ and $Y[f_m, k]$ is the received signal at m^{th} subcarrier. Then, feedback bit for each subcarrier is decided by comparing $\angle g[f_m, k]$ with the predefined constant α and incrementing beamforming gains accordingly as

$$\theta^n_{best}[f_m, k+1] = \begin{cases} \theta^n_{best}[f_m, k] + \gamma & \angle g[f_m, k] > \alpha \\ \theta^n_{best}[f_m, k] & otherwise \end{cases} . \tag{2.9}$$

That is, while the one bit feedback algorithm is adapting the phases at each subcarrier to achieve beamforming gain, we are running a consensus-style algorithm on the received

phases to attain phase continuity across subcarriers. However, instead of directly comparing phases, we work with complex amplitudes in order to avoid phase wrapping issues, and to provide a soft averaging mechanism in which subcarriers with larger received amplitudes have larger weight. The resulting net channel response of the 2-bit feedback algorithm is shown in Figure 2.3(c) for 10 transmitters beamforming over a dispersive channel with delay spread of $4.7\mu s$ using 1024-subcarrier OFDM with frequency spacing of 9.76kHz. It can be seen that the channel phase response is smooth. The amplitude remains equal to the amplitude provided by beamforming (i.e. equal to the sum of the channel amplitudes of all transmitters), since the one bit feedback algorithm operates in parallel to the phase smoothing mechanism using the second bit. The diversity provided by pooling the power of 10 transmitters significantly decreases frequency selectivity relative to both a single transmitter and noncoherent power pooling

2.4 Performance Analysis

Figure 2.4 shows the progress of net received signal power (summed over subcarriers) with time for 10 transmitters. We vary the SNR per user at the receiver across curves, keeping the transmit power the same. The initial condition for the algorithm is non coherent power pooling, and the progress towards the ideal beamforming solution depends on the noise level. We see that the 2-bit algorithm is fairly robust to noise, and enables reliable operation in regimes where a single transmitter would not be able to close the link without going to very low spectral efficiencies. However, there is some noise threshold beyond which the algorithm breaks down. For example, even when the SNR per user is as low as -5 dB, we do attain a significant fraction of the beamforming gain, but when the SNR per user dips to as low as -10 dB, we barely progress beyond noncoherent power pooling. We conjecture that this threshold effect is based on how large the power-pooled

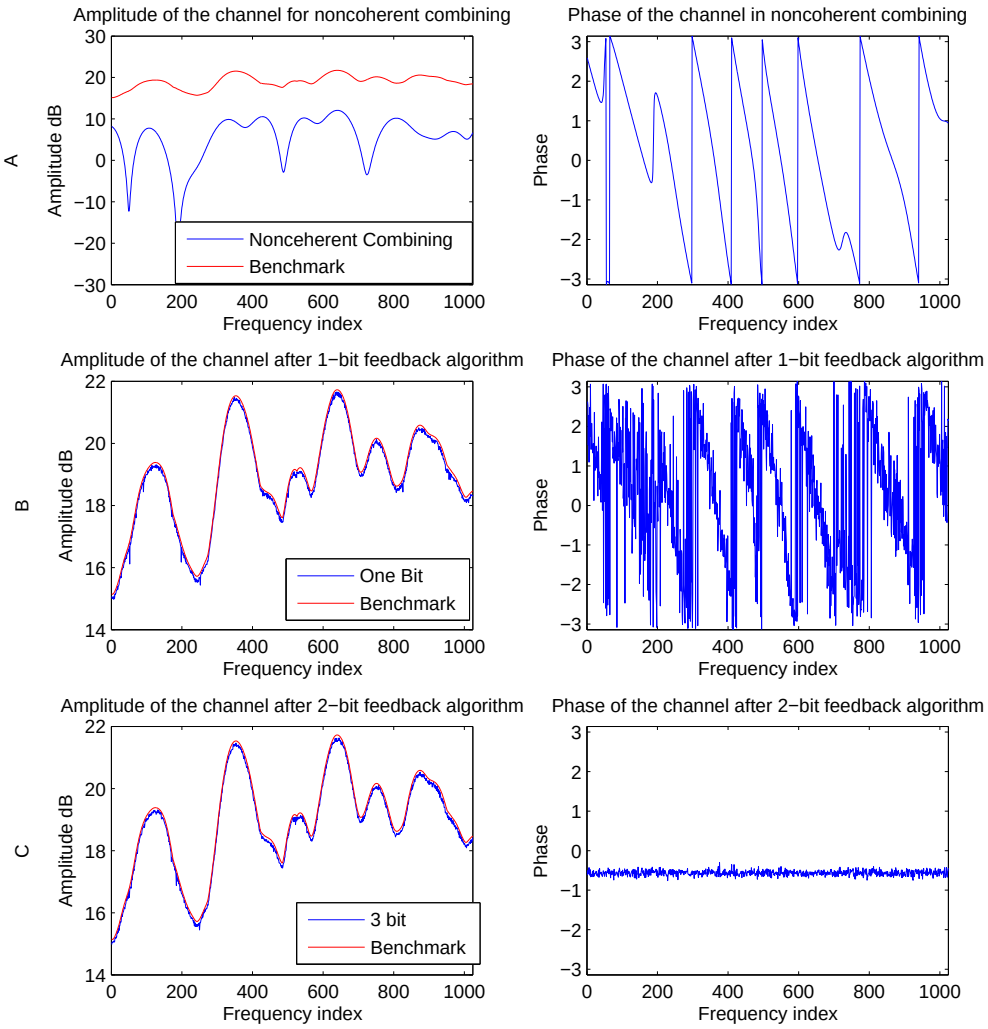

Figure 2.3: Amplitude and phase of net channel response of 10 transmitter for A) non–coherent combinations, B) coherent combination after convergence of 1-bit feedback, C) coherent combination and smoothing with 2-bit feedback

SNR that we bootstrap with is, but more analysis and performance evaluation will be presented in the next chapter.

The benchmark for perfect beamforming gain is shown in Figure 2.3(c) along with the net channel amplitude after beamforming for comparison. This value is calculated in (2.10) for subcarrier frequency f_m as:

$$|H_{opt}(f_m)| = \sum_{n=1}^{N} |H_n(f_m)| \tag{2.10}$$

where M is the number of transmitters and m is the transmitter index. In the proposed scheme, the process of channel smoothing is performed independently from beamforming, i.e. based on the smoothing feedback all transmitters apply the same phase rotation in each subcarrier causing a rotation in the net channel phasor but leaving its amplitude unchanged and beamforming gain unaffected. Consequently, the performance of 2-bit beamforming with OFDM modulation is identical to the basic 1-bit feedback procedure in a narrowband link, hence the speed of convergence, as seen in Figure 2.4, is similar to the predictions of [3] for the basic 1-bit feedback algorithm. For noiseless feedback, using optimum phase perturbation increment size of 9 degrees (obtained from simulations), 75% of beamforming gain is obtained after $5M = 50$ iterations. This step size, however, may not be optimal in the noisy settings considered here, and analysis of the one bit feedback algorithm under noise is further investigated in next chapter.

Receiver channel estimation: The resulting channel after convergence is relatively smooth and can be estimated by the receiver from a subset of subcarriers. In the LTE standard, channel estimation is performed at the receiver by interpolating the channel measured from a number of pilot subcarriers. One in six subcarriers are allocated for pilot transmission and channel sounding and the remaining subcarriers are used for data transmission. The net channel after convergence of 2-bit feedback is smooth in phase and relatively

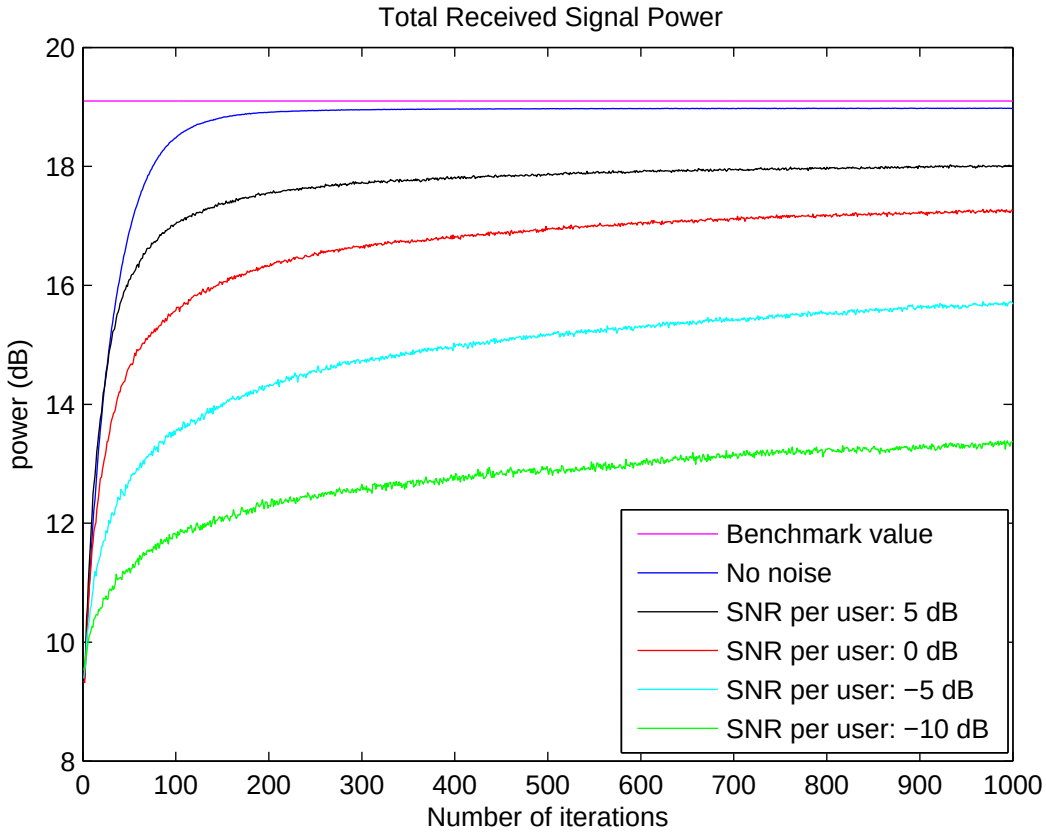

Figure 2.4: Convergence of 2-bit feedback with time

smooth in amplitude therefore channel estimations obtained by interpolation between one every seven subcarriers is low. The variation of interpolation error with iteration time is shown in Figure 2.5.

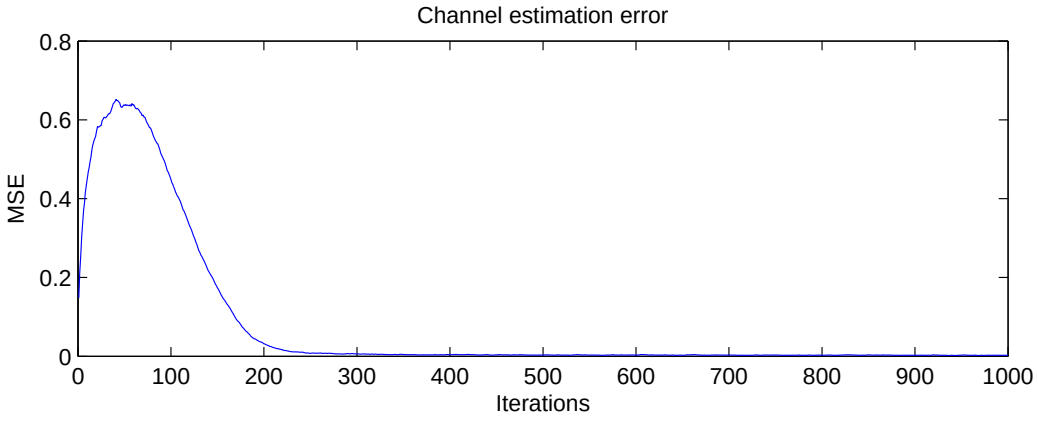

Figure 2.5: MSE of interpolation of channel estimate from subset of subcarriers

Chapter 3

Analysis of One Bit Feedback Algorithm in the Presence of Noise

In this chapter, we investigate the effect of the additive white Gaussian noise (AWGN) on the one bit feedback algorithm, with the goal of answering the following: can we operate in a regime in which SNR per node is made arbitrarily small by scaling up the number of nodes N. As illustrated in the previous chapter in Figure 2.4, the one bit feedback algorithm fails to progress beyond noncoherent power pooling gain at low SNR regimes. This regime is particularly interesting for distributed beamforming applications aiming for range extension.

The one bit feedback algorithm perturbs the phases of each transmitter at each step. The receiver broadcasts feedback based on the noisy received samples. The decision based on noisy samples requires modification on the one bit feedback algorithm, with the receiver performing noisy RSS comparisons over a window to avoid deadlocks due to noise. This iterative process is modeled as a Markov chain with transition probabilities computed using a Gaussian approximation for random variables associated with the RSS and its one-step evolution, similar to [33]. We perform a drift analysis on the RSS and

compute the fraction of the ideal beamforming gain that the algorithm converges to, and compare these analytical estimates with simulation results. We conclude that the effect of the noise cannot be countered by simply increasing N.

We use the narrowband system model as in (1.1). It is convenient to express phases taking as reference the direction of the received sample. Setting $\phi_i = \theta_i + \gamma_i + \psi_i - \angle(Z)$, we can write

$$Y = \left| \sum_{i=1}^{N} a_i e^{j\phi_i} + w \right|, \tag{3.1}$$

where $w \sim CN(0, N_0)$: the statistics of the noise are unchanged under the change of phase reference due to circular symmetry.

3.1 One bit feedback algorithm with memory

The one bit algorithm in a noisy setting is described as follows. The feedback $F(k)$ broadcast by the receiver at the end of time slot k is generated by comparing the current RSS with the best RSS from among the last M iterations, as follows.

$$F(k) = \begin{cases} 1 & Y(k) > Y_{best}(k) \\ 0 & Y(k) < Y_{best}(k) \end{cases}, \tag{3.2}$$

where

$$Y_{best}(k) = \max_{k-M \le t < k} Y(t)$$

Each transmitter updates its phase according to the feedback from receiver as follows.

$$\theta_i(k+1) = \begin{cases} \theta_i(k) & F(k) = 0 \\ \theta_i(k) + \delta_i & F(k) = 1 \end{cases}. \tag{3.3}$$

The one bit algorithm originally analyzed in a noiseless setting in [5] considers $M = \infty$

(i.e., the current RSS is compared against the best RSS seen so far). This can be problematic in our noisy setting if the receiver observes a noisy RSS value that is higher than the noiseless RSS from the current set of beamforming phases alone. This can cause the algorithm to get stuck, with actual improvements in beamformed RSS going unnoticed unless the improvement is higher than the deviation due to noise. We therefore require a windowing mechanism to enable forgetting such outliers due to noise.

3.2 Analysis of One Step Progression of Received Signal Strength

Our goal is to characterize the progression of the RSS in a noisy setting, and to estimate the value at which it saturates. We do this by estimating the expected change, or drift, in RSS over a single iteration, and finding the point at which this drift becomes zero. We model algorithm dynamics associated with windowing as a Markov chain, depicted in Figure 3.2 and discussed in more detail later, with the state at time t equal to S_i if the maximum RSS over the current window was observed at time $t - i$. The transition probabilities for this Markov chain model depend on the statistics of the noisy and noiseless RSS before and after phase perturbations over one step of the algorithm, and are characterized using jointly Gaussian approximations (which are found to be accurate even for moderately large N).

Consider the noisy and noiseless RSS values at a given iteration k (suppressed from the notation). Assuming channel gains $a_i = 1$ for simplicity, define the noiseless and noisy normalized RSS values (normalized by the maximum value of N) before phase

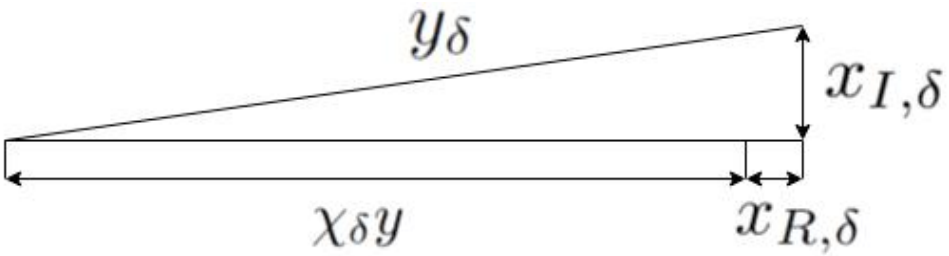

Figure 3.1: Effect of random phase perturbations on the total received signal

perturbation as

$$y = \frac{1}{N}Y = \frac{1}{N}|\sum_{i=1}^{N} e^{j\phi_i}|$$
$$y_n = \frac{1}{N}Y_n = \frac{1}{N}|\sum_{i=1}^{N} e^{j\phi_i} + w_1|$$

The corresponding noiseless and noisy normalized RSS values after random phase perturbations are applied at transmitters are given by

$$\begin{aligned} y_\delta &= \frac{1}{N}|\sum_{i=1}^{N} e^{j(\phi_i+\delta_i)}| \\ y_{\delta n} &= \frac{1}{N}|\sum_{i=1}^{N} e^{j(\phi_i+\delta_i)} + w_2|, \end{aligned} \tag{3.4}$$

where w_1, w_2 are i.i.d. $CN(0, N_0)$, and $\{\delta_i\}$ are i.i.d. (distribution specified later).

Following the approach in [5], conditioned on the normalized noiseless RSS y prior to phase perturbation, the evolution of normalized RSS is illustrated in Figure 3.1. For large N, application of the central limit theorem allows us to model the real and imaginary parts of the increments as independent Gaussian. Furthermore, the imaginary part of the increment (orthogonal to the current direction of the received sample) can be neglected,

yielding the approximation [5]

$$y_\delta \approx \chi_\delta y + x_{R,\delta} \tag{3.5}$$

where $\chi_\delta = \mathrm{E}[cos\delta_i]$ and $x_{R,\delta} \sim N(0, \sigma_\delta^2)$ with variance

$$\sigma_\delta^2 = \frac{1 - \chi_\delta^2 - \rho_\delta \kappa(y)}{2N} \tag{3.6}$$

where

$$\rho_\delta = \chi_\delta^2 - \mathrm{E}[cos(2\delta_i)], \quad \kappa(y) = \frac{I_2(m)}{I_0(m)} \tag{3.7}$$

and m is derived from

$$y = \frac{I_1(m)}{I_0(m)} \tag{3.8}$$

where I is the modified Bessel function of the first kind.

It now becomes possible to approximate the noisy RSS simply by adding the real part of the noise sample to the noiseless RSS:

$$\begin{aligned} y_n &\approx y + w_{R,1} \\ y_{\delta n} &\approx \chi_\delta y + x_{R,\delta} + w_{R,2} \end{aligned} \tag{3.9}$$

where $w_{R,1}$ $w_{R,2}$ are the real parts of w_1/N and w_2/N, and are therefore modeled as i.i.d. $N(0, \sigma_n^2)$, with variance $\sigma_n^2 = \frac{N_0}{2N^2}$.

The receiver knows the one-step change in the noisy RSS, given by $U \triangleq y_{\delta n} - y_n$, whereas we would like to make decisions based on the one-step change in the noiseless RSS, given by $V \triangleq y_\delta - y$. Under our approximations (3.5) and (3.9), U and V are jointly

Gaussian:

$$\begin{bmatrix} U \\ V \end{bmatrix} \sim N\left(\begin{bmatrix} (\chi_\delta - 1)y \\ (\chi_\delta - 1)y \end{bmatrix} \quad \begin{bmatrix} \sigma_\delta^2 + 2\sigma_n^2 & \sigma_\delta^2 \\ \sigma_\delta^2 & \sigma_\delta^2 \end{bmatrix} \right). \tag{3.10}$$

As described shortly, we use such joint Gaussian approximations to compute the transition probabilities for the Markov chain modeling the algorithm dynamics.

Note that, in [5] it has been shown that the optimal choice for δ_i is a distribution with variance scaling as $1/N$. Thus, we choose phase rotations from uniform distribution $\delta_i \sim U(-c/\sqrt{N}, c/\sqrt{N}]$, where c is a constant chosen based on simulation. This is easily seen to imply that $\sigma_\delta^2 \sim \frac{1}{N^2}$, which is the same scaling as the noise variance σ_n^2. Thus the entries of the covariance matrix in (3.10) scale with $1/N^2$, with the relative strengths of the phase perturbation and noise terms being independent of N.

3.3 Performance Analysis with Received Signal Strength Memory

In order to compute expected value of the RSS drift given noiseless RSS value y, we make the simplifying assumption that RSS drift at iteration k is statistically independent of the feedback before $k - M$.The RSS drift at the kth step conditioned on current state S_m and noiseless RSS value y with memory size M can be written as

$$\text{Drift}(RSS_k | S_m, y) = \mathbb{E}[V_k | \text{ feedback since } k - m, y]. \tag{3.11}$$

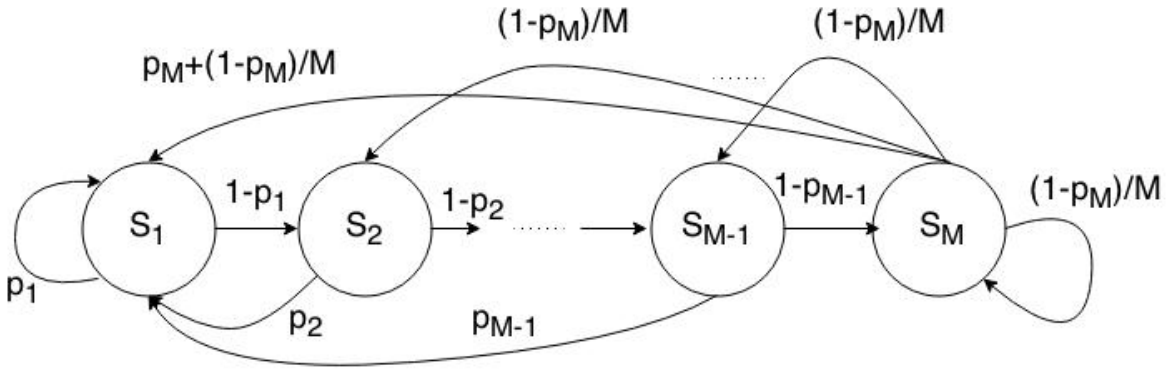

Figure 3.2: Markov chain

The total RSS drift with memory size M can be computed as

$$\text{Drift}(RSS_k|y) = \sum_{m=1}^{M} \mathbb{P}(S_m|y) \cdot \text{Drift}(RSS_k|S_m, y). \tag{3.12}$$

The conditional drift in (3.12) can be expressed as:

$$\begin{aligned} &\text{Drift}(RSS_k|S_m, y) = \\ &\quad \mathbb{P}(U_k > 0|S_m)\text{Drift}(RSS_k|S_m, U_k > 0, y) \\ &\quad +\mathbb{P}(U_k < 0|S_m)\text{Drift}(RSS_k|S_m, U_k < 0, y). \end{aligned} \tag{3.13}$$

We model the progress of the algorithm with the Markov chain shown in Figure 3.2. A positive feedback causes a transition to S_1 from any state. Negative feedback causes a transition from S_i to S_{i+1}, except when the final state is S_M. When we get negative feedback in state S_M, we assume that we transition to any of the M states with equal

probability. The state transition probability matrix can therefore be written as

$$\mathbf{P} = \begin{bmatrix} p_1 & 1-p_1 & 0 & \cdots & 0 \\ p_2 & 0 & 1-p_2 & \cdots & 0 \\ \vdots & \vdots & 0 & \ddots & \vdots \\ p_{M-1} & 0 & \ddots & 0 & 1-p_{M-1} \\ p_M + \frac{1-p_M}{M} & \frac{1-p_M}{M} & \cdots & \frac{1-p_M}{M} & \frac{1-p_M}{M} \end{bmatrix}$$

The state transition probabilities p_m are the probabilities of having positive feedback when the algorithm is in state S_m and can be defined as

$$\begin{aligned} p_m =& \mathbb{P}(U_k > 0 | S_m, y) \\ =& \mathbb{P}(U_k > 0 | U_{k-1} < 0, ..., U_{k-m+1} < 0, y) \end{aligned} \tag{3.14}$$

which can be computed from multivariate Gaussian random vector $[U_k, U_{k-1}, ..., U_{k-m+1}]^T$.

We define the probability of the algorithm being in state m conditioned on noiseless RSS value y as $\mathbb{P}(S_m|y)$. The steady state stationary distribution of the Markov chain is computed as the left eigenvector of $\mathbf{P}$ corresponding to eigenvalue of 1.

The positive feedback drift term in (3.13) is computed as

$$\begin{aligned} &\text{Drift}(RSS_k | S_m, U_k > 0, y)) \\ &\quad = \mathbb{E}(V_k | U_k > 0, U_{k-1} < 0, ..., U_{k-m+1} < 0, y). \end{aligned} \tag{3.15}$$

where we compute this expectation from the multivariate Gaussian distribution of

$$[V_k, U_k, U_{k-1}, ..., U_{k-m+1}].$$

The negative feedback drift term in (3.13) is 0 except when the algorithm is in state M

since phase rotations δ_i are discarded as receiver broadcasts a negative feedback. When the algorithm is in state M and negative feedback is received then a new RSS value is considered in the next iteration. RSS drift for state M can be expressed as

$$\begin{aligned}\text{Drift}(RSS_k|S_M, U_k > 0, y)) = &\mathbb{P}[\text{max noisy RSS at } k-r] \\ &\times\mathbb{E}[V_{k-r}|U_{k-r} < 0, \{U_i < U_{k-r}\}_{,\forall i\neq(k-r),i>k-M}] \\ &=\mathbb{E}(V_k|U_k < 0, U_{k-1} < U_k, ..., U_{k-M+1} < U_k, y).\end{aligned} \tag{3.16}$$

where we compute this expectation from multivariate Gaussian vector $[V_k, U_k, U_{k-1}, ..., U_{k-M+1}]^T$ using Monte Carlo integration.

The total expected RSS drift is computed by combining (3.12) and (3.13) where we use our computed values for state probabilities, state transition probabilities and expected drift values for a given state. We estimate the steady state value of the noiseless normalized RSS y as the value corresponding to the zero crossing point of expected RSS drift conditioned on y.

3.4 Numerical Results

In this section, we present simulation results for our proposed architecture and compare them with our analytical approximations.

Figure 3.3 shows that the simulated histogram of (U, V) corresponds closely to our joint Gaussian analytical approximation. As SNR decreases, the correlation of U and V decreases, and hence the probabilities of the receiver broadcasting the correct decision ($P[U > 0|V > 0, y]$ and $P[U < 0|V < 0, y]$) approach 1/2 (if U becomes conditionally independent of V, then these approach $P[U > 0|y] = P[U < 0|y] = \frac{1}{2}$.

Analytical computations for expected drift in different noise settings are plotted in

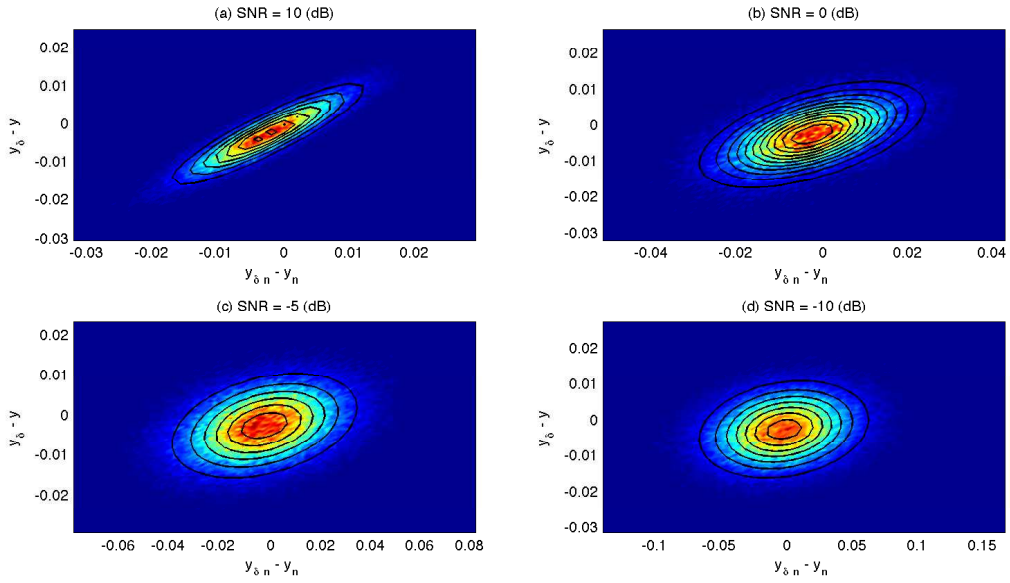

Figure 3.3: 2D histogram of noiseless versus noisy RSS increments ($N = 100$ transmitters and window size $M = 4$) compared against the analytical joint Gaussian distribution.

Figure 3.4. We see that the algorithm's progress is faster when the normalized RSS y is smaller, and that the steady state corresponding to the zero crossing values get worse as per-node SNR degrades.

Figure 3.5 shows simulation results for the normalized RSS values vs per-node SNR. These are "steady state" values obtained after $100N$ iterations, averaged over multiple runs, for different number of transmitters N. Random phase rotations are generated from uniform distribution $\delta_i \sim \mathcal{U}(-\Delta, \Delta)$ where $\Delta = 100/\sqrt{N}$. We observe that the normalized steady state RSS values from simulations match with the corresponding zero crossing values of expected RSS drift in Figure 3.4. The match between our analytical results and simulations does degrade slightly at lower SNR: the analytical results are pessimistic. However, the insensitivity of the steady state normalized RSS to N is indeed as predicted by the analysis.

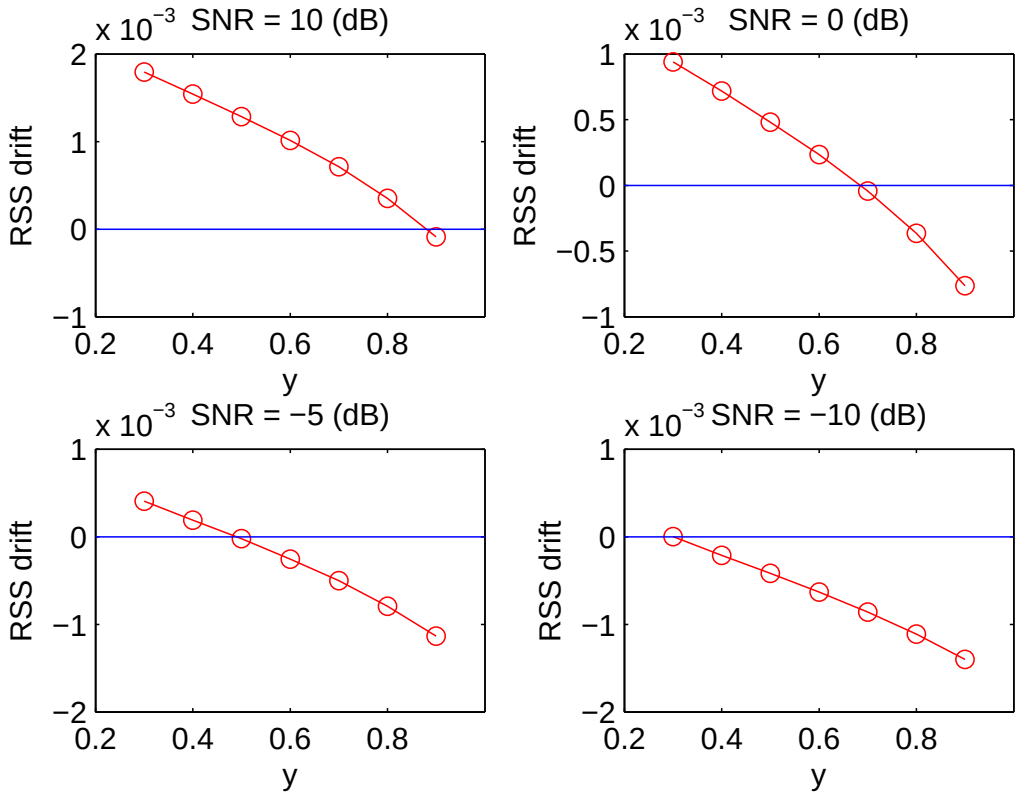

Figure 3.4: Theoretical values of RSS drifts with window size $M = 4$ and for $N = 100$ transmitters in different noise levels

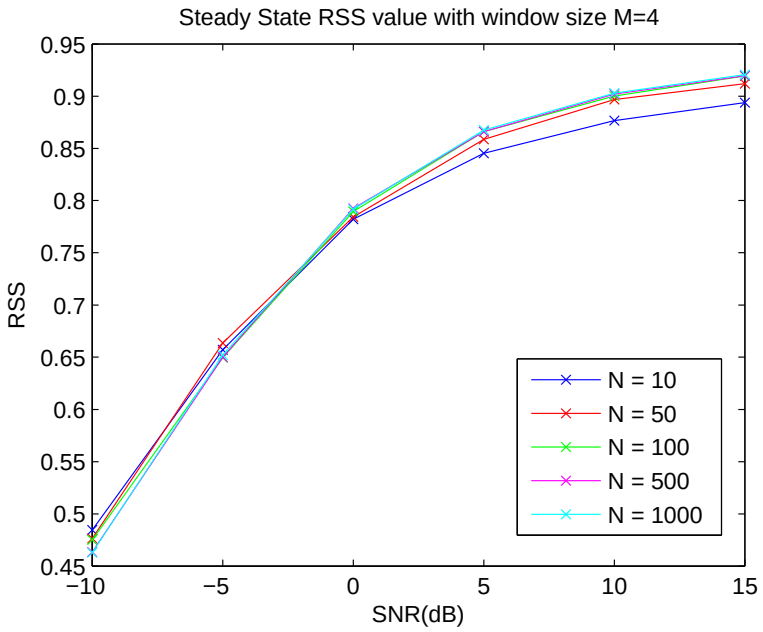

Figure 3.5: Simulated normalized RSS values vs SNR for different number of transmitters, RSS memory size $M = 4$ and random phase rotations $\delta_i \sim \mathcal{U}(-\Delta, \Delta)$

Chapter 4

Distributed Base Station

4.1 Introduction

In this chapter, we propose a training based distributed beamforming approach, termed deterministic orthogonal sequence training (DOST), designed to operate in low SNR regimes in which the one bit feedback algorithm and its variants fail, as shown in the previous chapter. We build on this algorithm to design of the DBS concept system, targeting significant improvements in communication link range and/or data rate. As shown in Figure 4.1, a DBS comprises N opportunistically placed, low-cost, transmitter nodes, without wired connections between the nodes. Our goal is to leverage the N^2-fold received power gain provided by distributed transmit beamforming to significantly enhance downlink range and/or spectral efficiency. We extend the DOST scheme to wideband system by simple interpolation across pilot subcarriers. We discuss pilot placement under different channel conditions. We compactly characterize downlink DBS performance with a outage capacity analysis. Finally, we note that feedback link may become a bottleneck in terms of the rate of channel time variations that can be supported. We use outage capacity analysis to provide insight on the system-level impact of

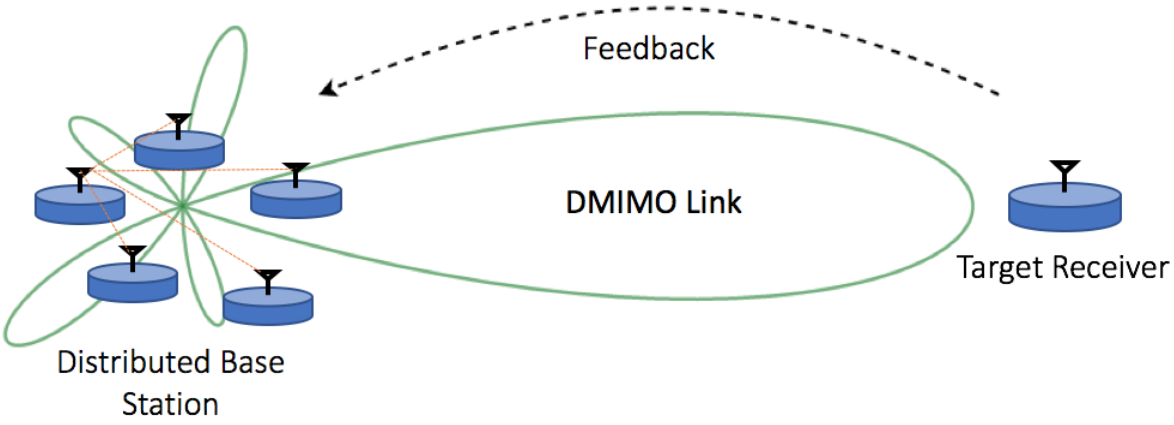

Figure 4.1: The Distributed Base Station Concept System.

the feedback link.

In practice, N coordinating nodes can obtain N-fold gain without beamforming with loose timing coordination between the transmitters (e.g., so the delay spread seen by the receiver across transmitters is smaller than the size of an OFDM cyclic prefix). Therefore, our proposed algorithm builds on this power pooling gain to bootstrap from a low-SNR regime to train beamforming weights.

As an example of the system enhancements possible with a 10-node DBS (our running example), consider a rural broadband link served by a single transmitter node in white space frequencies (50-800 MHz). For a receiver at the cell edge, which could only sustain a very low rate control channel at -5 dB SNR with a single base station transmitter, a 10-node DBS boosts the SNR at the receiver to 5 dB with power pooling, and to 15 dB with ideal beamforming. For typical SNR versus modulation and coding scheme (MCS) values for LTE adaptive modulation [34], we can sustain QPSK with rate 2/3 coding with power pooling, and 64QAM with rate 2/3 coding with beamforming. Thus, for a channel bandwidth of 20 MHz, a DBS makes it possible to provide broadband data rates of 20-80 Mbps at a range where a single transmitter system could barely establish a control link.

4.1.1 Related Work

With the increasing availability of low-cost front-end elements, architectures that take advantage of the degrees of freedom offered by massive deployment of antenna elements have gained in popularity. Acquisition of adequate channel state information at the transmitter (CSIT) is crucial for FDD massive MIMO systems. Traditional codebooks for channel feedback [35, 36] require the number of feedback bits to scale linearly with the number of BS antennas [37]. Efficient codebook design based on the channel statistics [38] and sparsity inspired approaches are proposed in [39, 40] to reduce feedback overhead. Explicit and heavily quantized feedback is key to achieve beamforming gain while preserving downlink resources. For instance, an LTE base station with 64 antennas would use approximately 48% of the downlink resources to send reference signals [41]. The fundamental differences between this body of work and our framework are as follows. First, in order for the network protocols to scale with the number of distributed transmitters, and to allow opportunistic expansion of the DBS, we constrain the receiver to be oblivious to the number and identity of transmitters. Thus, instead of performing channel estimation and then producing quantized feedback, the feedback must be based on the receiver's *aggregate* measurements. This still allows us to consider standard training strategies, in which different transmitters send orthogonal or quasi-orthogonal training sequences, but constrains the form of feedback the receiver can send back. This implies, for example, that the receiver cannot perform spatial channel estimation followed by codebook-based quantization, or exploit sparsity, unlike in existing feedback-based techniques in massive MIMO. Second, the impact of operating in the low per-node SNR regime has not been considered in prior work on massive MIMO feedback. This limitation on the feedback rate can fundamentally limit the channel coherence times that can be supported.

Map of this Chapter: We present the system and channel model for DBS in Section

4.2. In Section 4.3, we present the DOST algorithm, as well as alternative strategies for beamforming, and compare these algorithms with simulations over narrowband channels. In Section 4.4, we extend the beamforming algorithms to wideband settings by using a subset of the OFDM subcarriers as pilots. We discuss selection of pilot resources along with possible interpolation techniques. Finally, Section 4.5 presents DBS system frame structure and performance analysis with outage capacity results. It includes a discussion of the reliability and system-level impact of the feedback link with different possible feedback link reception techniques.

4.2 System and Channel Model

4.2.1 DBS system model

The nodes in the DBS depicted in Figure 4.1 cooperate to send a common message to a distant receiver over a noisy multipath channel. We consider OFDM with a set of subcarriers designated as pilots. The receiver broadcasts explicit aggregate feedback on the complex signals received on the pilot subcarriers. Each transmitter in the DBS uses this feedback to estimate its complex channel gains to the receiver on the pilot subcarriers, and interpolates these to estimate the channel gains on the data subcarriers. Each transmitter then adjusts its phase on each subcarrier to compensate for the channel phase, in order to align coherently at the receiver. The transmitters are assumed to be synchronized in time and frequency as in Chapter 2.2 system model.

4.2.2 Signal Model

We denote the channel from node i to the receiver on subcarrier k by the complex gain $H_i(f_k) = a_{ik}e^{j\psi_{ik}}$, and the receiver's phase offset relative to transmitter i by γ_{ik}.

Transmitter i applies phase control via a beamforming weight of $e^{j\theta_{ik}}$ on its kth subcarrier. The received signal, after multiplying by the conjugate of the unit-amplitude pilot symbol, is given by

$$R[f_k] = \sum_{i=1}^{N} a_{ik} e^{j(\theta_{ik}+\gamma_{ik}+\psi_{ik})} + w[k] \tag{4.1}$$

The corresponding normalized received signal strength (RSS) is given by

$$r[f_k] = \frac{|R[f_k]|}{N} \tag{4.2}$$

and is used as a performance metric to compare different beamforming algorithms.

The aim of distributed transmit beamforming is to maximize RSS. This is achieved when each transmitter chooses a beamforming phase that reverses its total offset relative to the receiver allowing all signals to combine coherently upon reception. The optimal solution is therefore $\theta_{ik} = -(\gamma_{ik} + \psi_{ik})$ up to a common constant shift across all nodes. The received RSS is then equal to

$$R_{\max}[f_k] = \sum_{i=1}^{N} a_{ik} \tag{4.3}$$

and the normalized RSS $r[f_k]$ approaches the maximum achievable value.

4.2.3 Channel Model

The multipath channel between a typical transmitter node and the receiver is modeled as

$$h(\tau) = \sum_{p=1}^{N_p} \alpha_p \delta(\tau - \tau_p)$$

where N_p denotes the number of paths, τ_p the delay and α_p the complex gain of path p. For concreteness, we consider Rayleigh fading on each path, setting $\alpha_p = A_p v_p$ where v_p

are i.i.d. complex Gaussian with distribution $CN(0,1)$ and A_p is the normalized square root of the power delay profile (PDP) such that $\sum_p A_p^2 = 1$.

The frequency response for such a channel is:

$$H(f_k) = \sum_p A_p v_p e^{-j2\pi f_k \tau_p}$$

For each frequency f_k, $H(f_k)$ is zero-mean complex Gaussian with variance $\sum_i A_p^2 = 1$. Thus, the channel responses of each transmitter at different frequencies are identically distributed but correlated random variables with distribution $H(f_k) \sim CN(0,1)$.

In our numerical results, we use the 3GPP Extended Pedesterian A (EPA) channel model parameters shown in Table 4.1 to generate channels for each node in the DBS [42]. Different nodes therefore have the same power-delay profile, but different channel realizations corresponding to i.i.d. draws of the $\{v_p\}$. We note that this channel model is not intended to provide a physical model of multipath components, but rather, may be viewed as a non-uniform tapped delay line representation of a bandlimited channel. We have also considered dithered versions of the delays for different nodes, and verified by simulations that the channel statistics in frequency domain do not change. Thus, the channel model should be viewed as a non-uniform tapped delay line representation, rather than a model for physical multipath components.

4.3 Narrowband Feedback-based Distributed Beamforming Techniques

In this section, we describe and justify our choice of training strategy through numerical comparison against alternative approaches. We focus on a narrowband system which serves as a model for a single pilot subcarrier in the wideband OFDM framework. As

Parameters			
Path Number	Delay (ns)	Relative Power (dB)	Fading
1	0	0.0	Rayleigh
2	30	-1.0	Rayleigh
3	70	-2.0	Rayleigh
4	90	-3.0	Rayleigh
5	110	-8.0	Rayleigh
6	190	-17.2	Rayleigh
7	410	-20.8	Rayleigh

Table 4.1: EPA channel model

mentioned, we are interested in techniques that scale well, in terms of both performance and protocol simplicity, as the number of transmitter nodes increases and as the received SNR per node approaches zero.

4.3.1 Deterministic Orthogonal Sequence Training

In this scheme, each node uses a predefined sequence of beamforming weights over L training transmissions and the L complex gains measured by the receiver are quantized and broadcast to the transmitters. By using orthogonal or quasi-orthogonal weight sequences on different nodes, each node can extract its channel from the feedback independently from other nodes.

Consider the $L \times N$ training matrix $\mathbf{A}$, the i'th column of which is the weight sequence used by node i. To design N orthogonal sequences, each sequence must be at least of length N, meaning the training period, which is equivalent to convergence time for the iterative approaches, is equal to N and scales linearly with array size. Using orthogonal sequences is then equivalent to choosing a training matrix for which $\mathbf{A}^H\mathbf{A}$ is diagonal. This orthogonality requires some coordination between transmitters to ensure one-to-one assignment of sequences to nodes. This requirement can be relaxed by using quasi-orthogonal pseudorandom sequences that nodes generate independently; the nor-

malized interference between sequences gets attenuated as their length grows. While it is possible to employ completely uncoordinated training by the latter choice, in practice, the coordination required for implementing truly orthogonal sequences (which provide the best possible performance for a given training duration and power) is minimal. There are many possible choices of training sequences, but for concreteness, we consider the DFT matrix in our results:

$$\mathbf{A} = \begin{bmatrix} 1 & 1 & \cdots & 1 & 1 \\ 1 & e^{-j2\pi/L} & \cdots & & e^{-j2\pi(N-1)/L} \\ \vdots & \vdots & \ddots & & \vdots \\ 1 & & & & \\ 1 & e^{-j2\pi(L-1)/L} & \cdots & & e^{-j2\pi(N-1)(L-1)/L} \end{bmatrix}$$

This is because DFT sequences are not only orthogonal, but they remain orthogonal when cyclically shifted by any amount. Thus, a transmitter can use any L-sized block of feedback to estimate its channel, without incurring interference from the sequences sent by the other transmitters. A receiver can therefore snoop on the pilot subcarriers at any time, and generate feedback for the transmitter nodes in the DBS. Similarly, any transmitter node can join or leave the DBS at any time, assuming basic OFDM frame alignment and frequency synchronization is maintained. This makes deployment and operation particularly simple.

The observations at the receiver, collected over times $l = 1, ..., L$, can be written as the $L \times 1$ vector

$$\mathbf{y} = \mathbf{A}\mathbf{h} + \mathbf{w}$$

where $\mathbf{h}$ is the $N \times 1$ channel vector across different transmitters and $\mathbf{w} \sim CN(0, N_0\mathbf{I})$ is the receiver noise.

The least squares estimate for the channel vector is given by

$$\widehat{\mathbf{h}} = \left(\mathbf{A}^H\mathbf{A}\right)^{-1}\mathbf{A}^H\mathbf{y} \tag{4.4}$$

assuming that $L \geq N$ and $\mathbf{A}$ has rank N. Each node can thus obtain its channel estimate by taking the inner product of its corresponding row in the matrix $(\mathbf{A}^H\mathbf{A})^{-1}\mathbf{A}^H$ and the channel measurement feedback vector.

The Cramer-Rao lower bound on error covariance is $\mathbf{C}_h = N_0\left(\mathbf{A}^H\mathbf{A}\right)^{-1}$. For each transmitter, the error covariance is bounded as

$$\mathrm{Var}(\hat{\mathbf{h}}_n) \geq (N_0(\mathbf{A}^H\mathbf{A})^{-1})_{n,n} \geq \frac{N_0}{(\mathbf{A}^H\mathbf{A})_{n,n}}$$

with the bound attained for orthogonal training (diagonal $\mathbf{A}^H\mathbf{A}$). In this case, each node can estimate its channel by separately correlating the observations with its own training sequence:

$$\hat{\mathbf{h}}_n = \frac{1}{L}\mathbf{a}_n^H\mathbf{y} = \mathbf{h}_n + \frac{1}{L}\mathbf{a}_n^H\mathbf{w} \tag{4.5}$$

where $\mathbf{a}_n$ is the nth column of the training matrix. The estimation error covariance $\mathrm{Var}(\hat{\mathbf{h}}_n) = N_0/L$ can be made arbitrarily small by increasing the training interval L. This also demonstrates the power-pooling advantage of the DOST algorithm; with L scaling linearly with N, the estimation accuracy improves as array size grows and longer links with lower RSS can be supported.

Quantization

In practice, the complex received signal amplitude measured at the receiver must be quantized to a limited number of bits and broadcast by the receiver. The variance of the received complex amplitude scales as N (the transmitted signals add up incoherently

during the training period), hence a natural question is whether the quantization resolution also needs to be enhanced as N increases. Fortunately, the answer is no: as long as the receiver scales its quantizer step size Δ as $\sqrt{N}$ to accommodate the amplitudes it is seeing, we can use a fixed number of quantization bins, and average out the quantization noise across the training period.

The channel estimate at transmitter n with quantized feedback can be written as

$$\begin{aligned}\hat{\mathbf{h}}_n &= \frac{1}{L}\mathbf{a}_n^{\mathbf{H}}(\mathbf{y}+\mathbf{n}_q) \\ &= \frac{1}{L}\mathbf{a}_n^{\mathbf{H}}\mathbf{y} + \frac{1}{L}\mathbf{a}_n^{\mathbf{H}}\mathbf{n}_q\end{aligned}$$

where $\mathbf{n}_q$ is the quantization noise vector. Assuming quantization noise is distributed uniformly over the span associated to each level, the variance of any element $n_q[l]$ of the quantization noise vector scales as

$$\mathrm{Var}(n_q[l]) = \frac{\Delta^2}{12} \sim N.$$

If the quantization noise values can be approximated as independent over time, we have

$$\mathrm{Var}(\frac{1}{L}\mathbf{a}_n^H\mathbf{n}_q) \sim \frac{NL}{L^2} = \frac{N}{L}$$

so that the effect of quantization noise on channel estimation can be made independent of N by scaling L linearly with N. Thus, we can use a fixed feedback rate even as we increase the number of transmitters N, as long as the length of the training period scales linearly with N.

4.3.2 Alternative Strategies

The goal here is not to be comprehensive, but to show that the proposed DOST strategy is better matched to the low-SNR regime than methods that have been suggested in the literature, and natural variants thereof. To this end, we consider per-node deterministic training, the one bit feedback algorithm as described in Chapter 3.1, and variants of the latter that employ 2 bits per iteration.

4.3.2.1 Successive Deterministic Distributed Beamforming

A special case of deterministic orthogonal training is time-multiplexed training where only one transmitter is active at a time and the phase offset measured at the receiver is fed back to individual nodes successively. This procedure, termed Successive Deterministic Distributed Beamforming (SDDB) in [43] and such a scheme has been successfully prototyped [44], corresponds to setting the training matrix to identity, i.e., $\mathbf{A} = \mathbf{I}_{NxN}$. As our analysis and numerical results demonstrate, this method is poorly matched to the low per-node SNR regime of interest to us, since a transmitter is not able to use the entire training period to average out noise. Of course, if the per-node SNR is large enough SDDB may be preferable in terms of power conservation as only one transmitter is active at any time during a training period of similar length. This may be the case for shorter range applications, in which the goal of distributed beamforming is to reduce transmitted power rather than to obtain range extension for a given transmitted power. On the other hand, SDDB is more resilient to quantization than DOST, since the dynamic range of the received signal is smaller when a single node is transmitting at a time.

4.3.2.2 Randomized two bit feedback algorithm (R2BF)

The authors in [12] propose a modified version of OBF, namely the randomized 2 bit feedback algorithm (R2BF), in order to speed up convergence. Assuming that the receiver has knowledge of the maximum possible RSS value obtained by perfect beamforming, the feedback bits are set as follows:

$$F[t] = \begin{cases} 11 & \text{if } R[t] > R_{\text{best}}[t] \text{ and close to } \text{RSS}_{\max} \\ 10 & \text{if } R[t] > R_{\text{best}}[t] \text{ half way from } \text{RSS}_{\max} \\ 01 & \text{if } R[t] > R_{\text{best}}[t] \text{ and far from } \text{RSS}_{\max} \\ 00 & \text{if } R[t] < R_{\text{best}}[t] \end{cases} \tag{4.6}$$

and the phase update (3.3) becomes

$$\theta_i[t+1] = \begin{cases} \theta_i[t] & \text{if } F[t] = 00 \\ \theta_i[t] + \delta_i[t] & \text{otherwise} \end{cases}$$

In the next time slot, $\delta_i[t+1]$ is chosen from a different distribution depending on the feedback, i.e. $\delta_i[t+1] \sim U[-\frac{\pi}{\beta}, \frac{\pi}{\beta}]$ where:

$$\beta = \begin{cases} \beta_1 & \text{if } F[t] = 01 \\ \beta_2 & \text{if } F[t] = 10 \\ \beta_3 & \text{if } F[t] = 11 \end{cases}$$

where $\beta_1 < \beta_2 < \beta_3$. This approach increases the convergence speed of 1BF by around 25%, but with the additional requirement of the receiver knowing the maximum RSS, which in turn requires knowledge of the number of transmitters and the channel statistics. This method therefore requires a higher level of coordination between nodes and is less robust and distributed.

4.3.2.3 Modified two bit feedback algorithm (M2BF)

We propose a different modification of one bit feedback, where the additional bit of feedback is used to quantify the *amount* of improvement obtained from the perturbations. The additional feedback bit relative to (3.2) is generated as follows:

$$F[t] = \begin{cases} 11 & \text{if } \alpha_1 \leq R[t] - R_{\text{best}}[t] \\ 10 & \text{if } 0 \leq R[t] - R_{\text{best}}[t] < \alpha_1 \\ 01 & \text{if } \alpha_2 \leq R[t] - R_{\text{best}}[t] < 0 \\ 00 & \text{if } R[t] - R_{\text{best}}[t] \leq \alpha_2 \end{cases} \tag{4.7}$$

where α_1 and α_2 are predefined constants dependent on channel statistics, but independent of N. If the RSS *improvement* from current random phase perturbations is above threshold α_1, all transmitters make use of this knowledge and apply the previous perturbations again in the next iteration. If the *degradation* caused by the perturbation is more than threshold α_2, the phases are reversed and transmitters perturb their phases in the opposite direction. Therefore $\delta_i[t+1]$ becomes dependent on the previous perturbation $\delta_i[t]$ as follows:

$$\delta_i[t+1] = \begin{cases} \text{new random} & \text{if } F[t] = 10 \text{ or } 01 \\ \delta_i[t] & \text{if } F[t] = 11 \\ -\delta_i[t] & \text{if } F[t] = 00 \end{cases} \tag{4.8}$$

4.3.3 Numerical results and comparisons

To evaluate and compare the beamforming performance and convergence speed of the preceding algorithms, we fix the number of feedback bits to 2 and plot the progression of each algorithm with the number of iterations. We compare DOST with 2-bit quantized feedback against the 2-bit SDDB, M2BF and R2BF strategies discussed above. While

our later system-level numerical results are for a DBS with 10 nodes, in this section, we consider a larger number of nodes ($N = 100$) in order to stress test the feedback strategies considered. We investigate the evolution of beamforming gain as a function of iterations using Monte Carlo simulations.

The distributed beamforming schemes used in the simulations have the following parameters: the phase perturbations $\delta_i[t]$ are generated from the uniform distribution $\mathcal{U}(-10°, 10°)$. R2BF uses $\beta_1 = 5°$, $\beta_2 = 10°$, $\beta_1 = 25°$ and constant thresholds of $\xi_1 = 0.3$, $\xi_2 = 0.8$ to decide from the R_{best} where RSS fits in (4.6). For M2BF, $\alpha_{1,2} = 0.8$ and the phase perturbations are designed to decay exponentially from $\mathcal{U}(-45°, 45°)$ with the number of iterations.

We first focus on understanding the effect of quantization in a noiseless setting. Figure 4.2 shows, at each iteration, the RSS level that would be obtained by nodes using their current channel estimate for beamforming. The curves of Figure 4.2 are the result of averaging over 2000 realizations of an $N = 100$ element array in a noiseless setting. For deterministic algorithms, training is stopped after $L = 100$ iterations, which constitutes one "batch" of training. In the absence of noise, the stochastic algorithms, R2BF and M2BF, converge asymptotically to optimal beamforming, while deterministic algorithms hit an performance gap of 1 and 2 dB away from optimal beamforming for SDDB and DOST, respectively, due to feedback quantization. When the feedback link is not a bottleneck, increasing the number of feedback bits can also be used to decrease quantization loss, but our interest is in the low per-node SNR regime, where this is not a feasible strategy. Thus, in a noiseless setting with severe feedback quantization, the one bit feedback algorithm and its variants actually perform better than deterministic training. And among the deterministic strategies, time-multiplexing across nodes as in SDDB is better than DOST, since the dynamic range of the received signal is smaller.

However, the picture is quite different when we consider the low per-node SNR regime

of interest to us. Figure 4.3 shows the evolution of the beamforming algorithms at per-node SNR of -5 dB. Since the SDDB scheme does not get the benefit of time averaging, it falls 7 dB short of the ideal 20 dB beamforming gain after N iterations, whereas DOST comes to within 2 dB of the ideal beamforming gain. The one bit beamforming schemes perform very poorly and we do not plot it. Among its two-bit variants, the M2BF scheme performs better than the R2BF scheme, but falls well short of the ideal beamforming gain: 8 dB lower after $N = 100$ iterations, and 5 dB lower even after 500 iterations. Thus, the DOST algorithm is by far the most resilient at low per-node SNR.

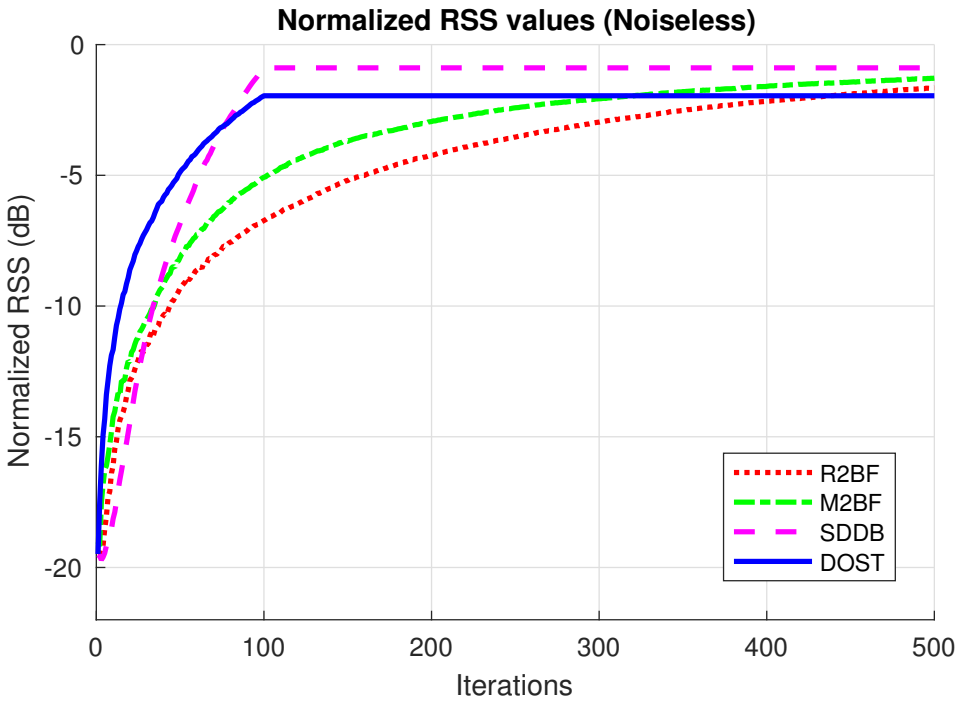

Figure 4.2: Evolution of the distributed beamforming approaches in a noiseless setting for $N = 100$ nodes

Impact of quantization

We now explore the impact of quantization further, by varying the number of bits of feedback per iteration in the DOST and SDDB algorithms. The number of feedback

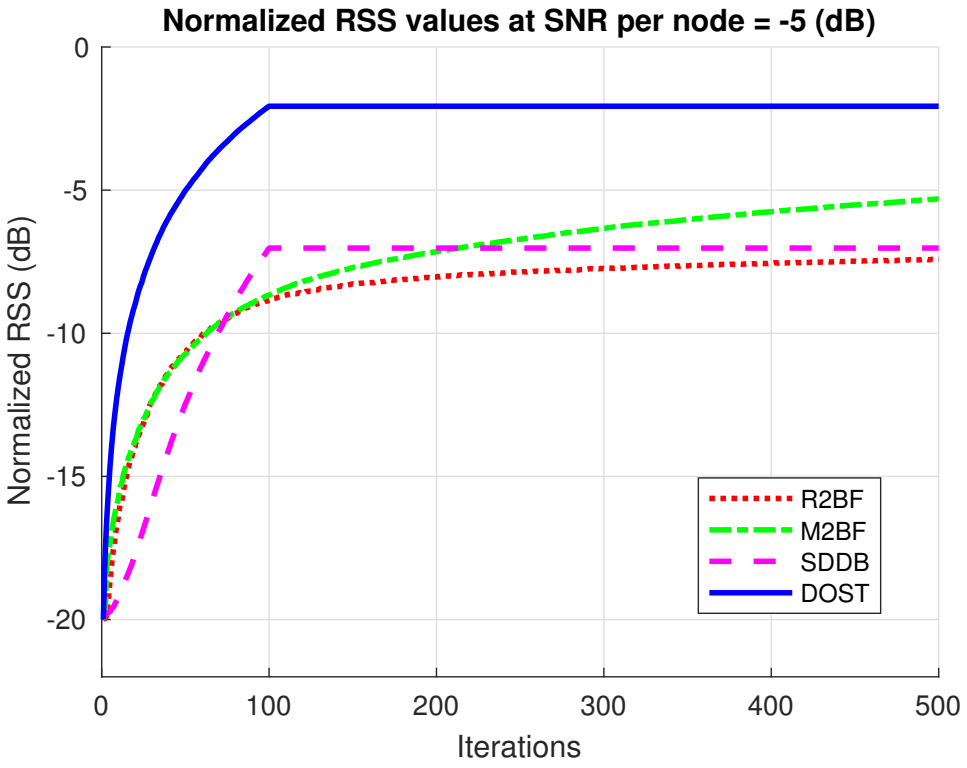

Figure 4.3: Evolution of the distributed beamforming approaches for $N = 100$ nodes at SNR per node -5 dB

bits is fixed to 2 for M2BF and R2BF, hence we do not consider those schemes here. Figure 4.4 shows the performance of the two algorithms with different levels of feedback quantization for different per-node SNR after 100 iterations of training. We consider 2-bit feedback quantization to quantize both real and imaginary parts of the received baseband signal. With 2-bit quantization, DOST is able to achieve within 2 dB of the ideal solution. Increasing the number of quantization bits to 4 bits improves both algorithms by around 1 dB and further increasing it to 6 bits gives very slight performance improvement. These results show that DOST can achieve near-optimal beamforming gains with heavily quantized feedback, as low as 2 bits per iteration, making it competitive with stochastic ascent approaches like R2BF and M2BF, even in noise-free conditions where they perform best.

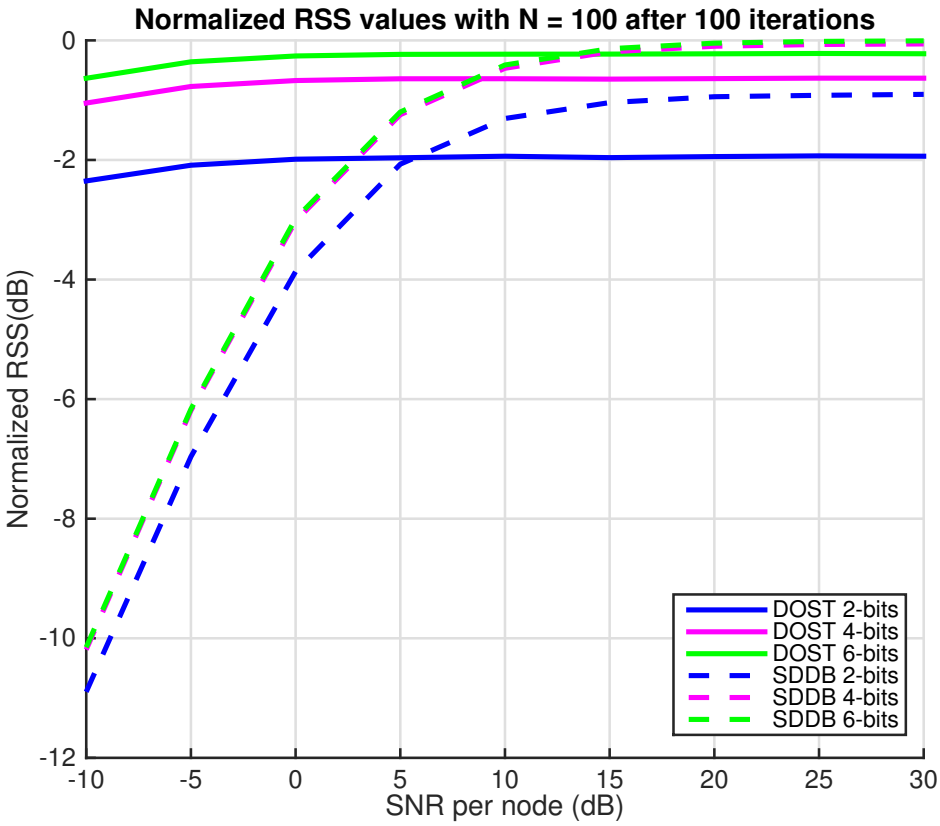

Figure 4.4: Normalized beamforming gains for SDDB and DOST for different number of feedback bits

4.4 Extension to Wideband using OFDM

4.4.1 Using simple interpolation

To extend the framework to wideband, an OFDM framework is utilized wherein DOST is applied on a subset of the OFDM subcarriers by placing training pilots at known positions in the OFDM symbol grid. Different pilot placements are possible for the training, including the block type, the comb type, or 2D-grid type [45]. In a block type arrangement, the pilots are placed on all subcarriers in a few OFDM symbols; in the comb type, the pilots are present in all OFDM symbols over a subset of subcarriers as shown in Figure 4.5; and in the 2D-grid type, the pilots are present in a subset of

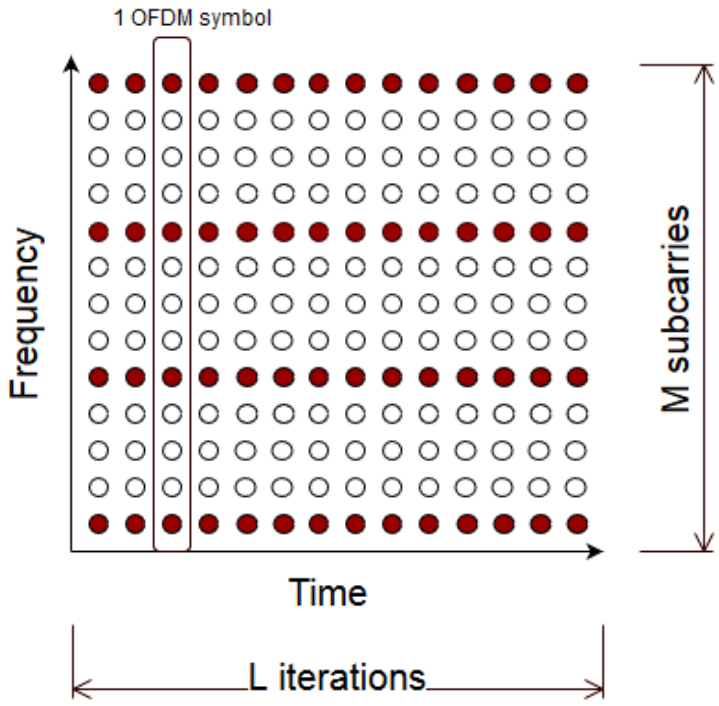

Figure 4.5: Proposed comb type pilot arrangement for channel estimation over OFDM grid

OFDM symbols over a subset of subcarriers. Therefore, the number of pilots in the 2D-grid pattern are less than the block and comb type pilot arrangements. Our goal here is to learn the channel as quickly as possible, hence for any given subcarrier, it is best to concentrate our pilot resources in time (over $L \geq N$ successive OFDM symbols for an N-node DBS) so as to get the required feedback from the receiver as quickly as possible. This is particularly important for maximizing the rate of channel time variations a DBS can support, because of the relatively low rate of feedback available on the uplink (see Section 4.5). However, by exploiting the continuity of the channel across frequency, we only need to employ pilots for a subset of subcarriers, and estimate the optimum beamforming weight for all other subcarriers via interpolation in the frequency domain. We therefore consider the comb type pilot arrangement shown in Figure 4.5 for the DBS deployment.

A number of different interpolation strategies can be used to extend the pilot subcar-

rier channel estimates to the remaining subcarriers, including linear interpolation, second order interpolation, low pass interpolation, spline cubic interpolation, and time domain interpolation. We consider lowpass interpolation, which has been shown to work better with comb type pilots [45].

The typical LTE system parameters shown in Table 4.2 are used in the simulations; and comb type pilots are placed at all OFDM symbols on a subset of 200 equispaced subcarriers. The minimum required number of OFDM symbols for training is $L \geq N$, and the minimum required time for training is 0.71 ms for $N = 10$ nodes. Note that a standard 2D grid type pilot arrangement, as illustrated in Figure 4.6, would require a longer training time. For the system parameters of Table 4.2, the minimum required number of OFDM symbols for training is also $L \geq N$, however, a subset of OFDM symbols are used as the pilots and the required time for training is $7L$ OFDM symbols which corresponds to a minimum training time of 5 ms for $N = 10$ nodes. This gap grows linearly with the number of nodes and can become a bottleneck when scaling to larger arrays.

Variables	Parameters
Number of nodes (N)	10
Bandwidth (Downlink)	20 MHz
Bandwidth (Uplink)	20 MHz
Number of subcarriers	1200
Number of pilot subcarriers	200
Size of FFT	2048
Subframe length	1 ms
OFDM symbols per subframe	14
Channel Model	EPA
Doppler Spread	5 Hz

Table 4.2: Link Level System parameters

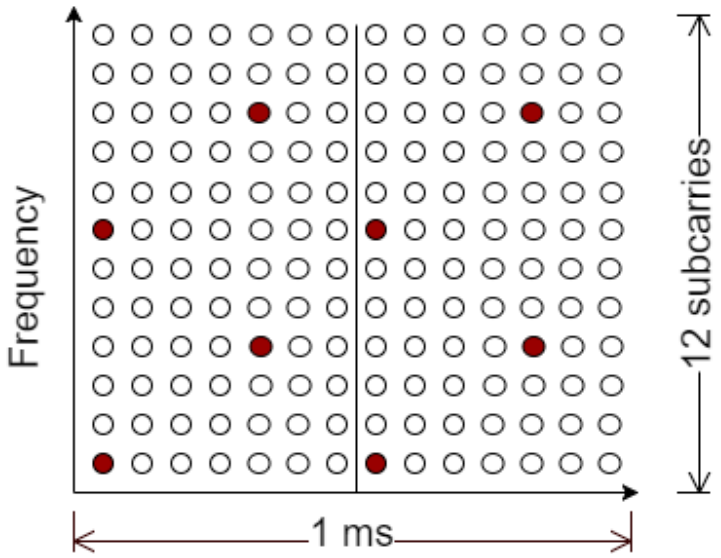

Figure 4.6: Standard 2D-grid type pilot placement is not well matched to a DBS OFDM downlink.

4.4.2 Using time-domain sparsity

The DOST algorithm is extended to OFDM over wideband channels by employing training on a subset of subcarriers, as shown in Figure 4.5. The channel estimates over the training subcarriers are interpolated to all subcarriers by first performing a sparse time domain channel reconstruction. In particular, we assume that the time domain channel is modeled as a discrete multipath channel:

$$h_n(t) = \sum_{k=1}^{K} g_k \delta(t - \tau_k) \tag{4.9}$$

In the frequency domain, this channel is a mixture of sinusoids with "frequencies" equal to multipath delays:

$$H_n(f) = \sum_{k=1}^{K} g_k e^{-j2\pi f \tau_k} \tag{4.10}$$

The problem of reconstructing the channel from estimates at a subset of subcarriers is therefore equivalent to finding the frequency (τ_k) and amplitude (g_k) of each sinusoid

in the mixture. In order to solve this problem, we use a dual of a frequency estimation algorithm developed in [46]. The inputs are the channel measurements $\hat{H}_n(f_i)$ on the training subcarriers. The outputs are estimates of the multipath delays and complex amplitudes. These estimates are then substituted in (4.10) to obtain channel estimates (and hence beamforming weights) for all subcarriers.

At low SNR per node and severe quantization, the frequency estimation algorithm used to detect delay components can overfit by producing spurious low-amplitude taps with delays larger than the channel delay spread. We find that channel estimates are improved by a simple denoising procedure which excludes these components. One realization of a 5-tap time domain channel is shown in Figure 4.7 along with the estimated taps using channel estimates at 32 out of 256 subcarriers. The channel estimates were obtained using the DOST algorithm in a 20 element array over training time of 100 iterations. The phase of the reconstructed channel, consisting only of the first 5 estimated taps with estimated delays smaller than the channel delay spread of $1/\Delta f = 1\mu s$, is shown in Figure 4.7 alongside the correct channel phase. It can be seen that the channel phase profile across frequency is estimated accurately even at a low per-node SNR of -10 dB and drastic quantization of 1 bit per I/Q dimension (or equivalently, four-phase quantization).

4.4.3 Simulation results

Simulation results using uncorrelated EPA channels with the power delay profile of Table 4.1 and system parameters of Table 4.2 are reported here for the wideband setting. The comb type pilot arrangement is used with subcarrier spacing of 6. Figure 4.8 shows the performance of beamforming algorithms averaged over subcarriers for $N = 10$ nodes. DOST achieves within 3 dB of the ideal solution, and works better than SDDB at low

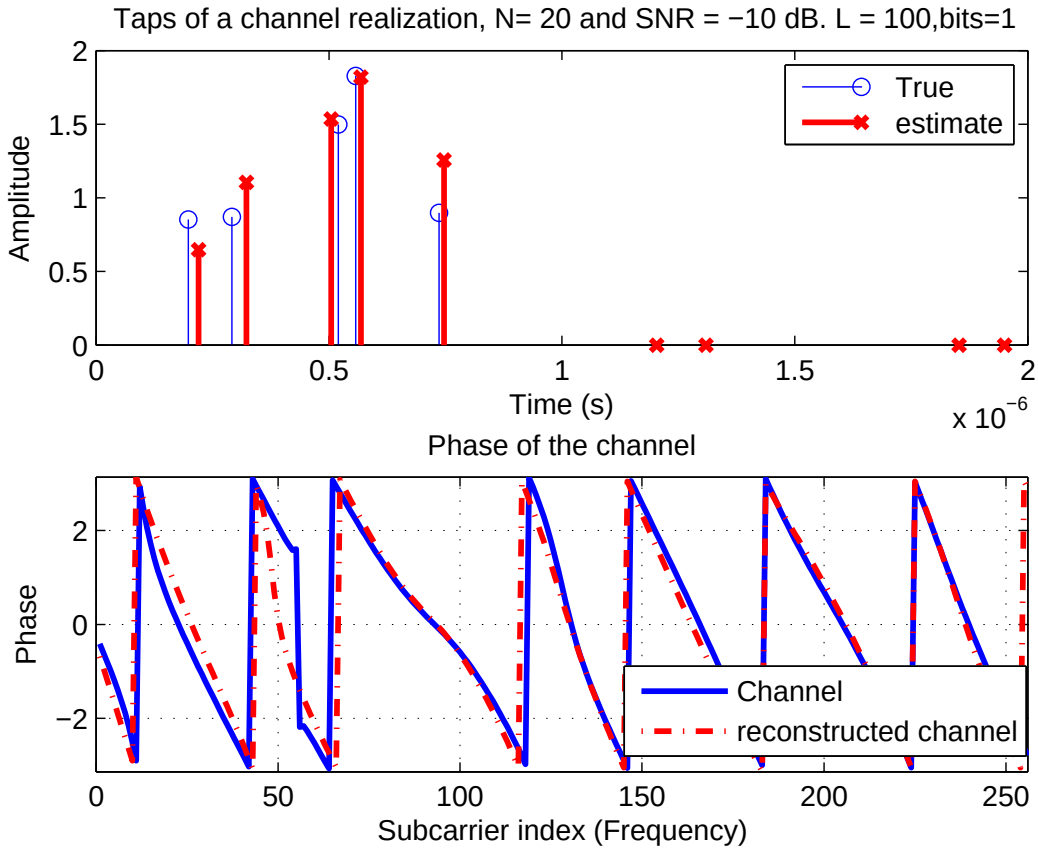

Figure 4.7: A realization of time domain channel estimation algorithm using subset of subcarriers (32 out of 256) and reconstructed phase of the channel by time domain estimates

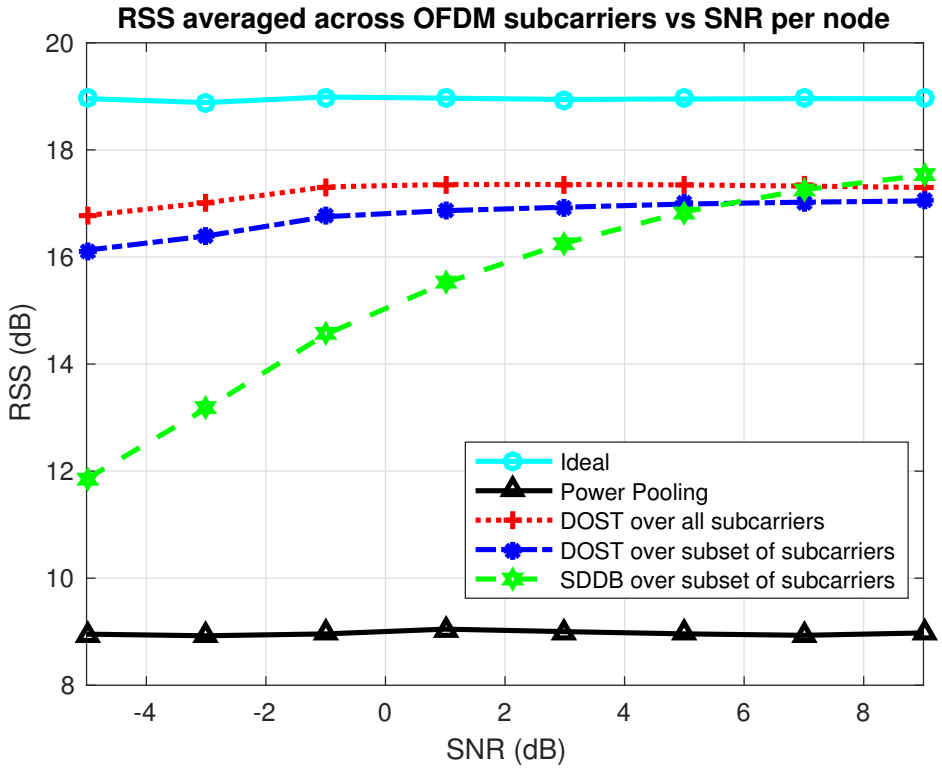

Figure 4.8: RSS averaged over OFDM subcarriers vs SNR per node for $N = 10$ nodes

per-node SNR. The degradation due to interpolation of comb type pilots is only 0.5 dB compared to a setting in which all subcarriers are used as pilots.

4.5 System Performance

We now provide performance characterization via outage rates for the downlink transmission of pilots and data and for feedback broadcast in the uplink direction. For simplicity, we use the terms "capacity" and "outage rate/capacity" to denote spectral efficiencies, either for a narrowband system (modeling a single subcarrier), or averaged over subcarriers for a wideband system. We use the term "data rate" when we multiply such spectral efficiencies by the bandwidth.

The forward link enjoys the benefits of N-fold power pooling gain during training, and

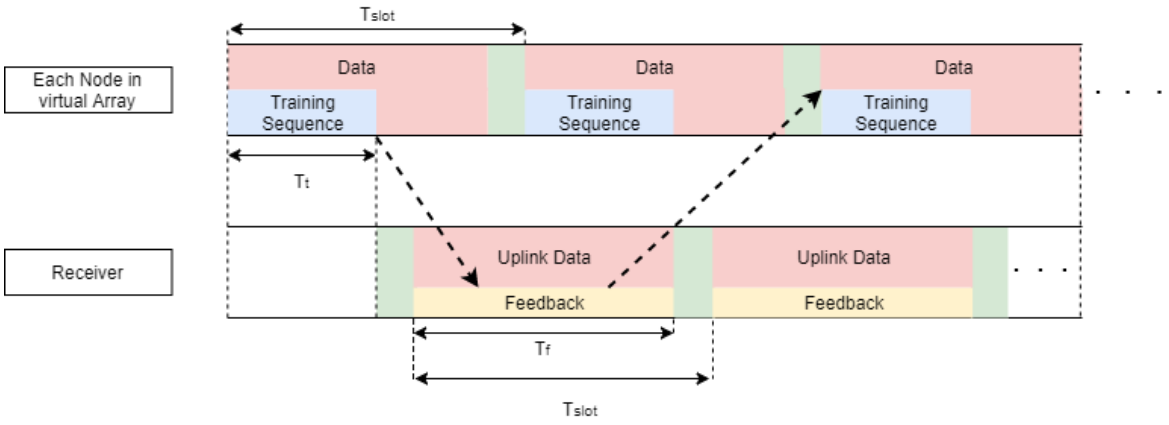

Figure 4.9: DBS frame structure with a slow feedback link.

N^2-fold distributed transmit beamforming gain during post-training data transmission. The rate of the feedback link depends on the sophistication of its reception strategy, as well as its allocated resources, which may be less than that of the forward link. There is no power pooling on the uplink and transmission is at an N-fold disadvantage in this direction relative to downlink. This asymmetry may be offset by using distributed receive beamforming in the feedback direction to pool the resources of the array and allow uplink scaling to keep up with downlink. Different analog and digital receive beamforming algorithms have been proposed in previous works such as [33, 47]. In the worst case, however, feedback is delivered over a SISO channel, either by having each node decode and use the feedback independently or use a single designated node for feedback reception. In this case, if the downlink power emitted by a single node in the DBS cluster and the uplink power emitted by the user node are comparable, then the feedback link may well be the scaling bottleneck and necessitate longer symbol durations to build up SNR, which will limit the rate of channel time variations that can be supported by the distributed array.

Figure 4.9 illustrates an example frame structure. During the startup phase, data

could be sent in power pooling mode at lower spectral efficiency, while sending training on the pilot subcarriers. Beamforming can be applied once the feedback corresponding to the pilots has been received. Once continuous communication has been established, feedback regarding the designated set of pilot subcarriers on the downlink in frame f is sent back during the next frame $f+1$, and the results are applied for distributed transmit beamforming in frame $f+2$. With such a scheme, for the first and second frames, data could still be sent in power pooling mode at lower spectral efficiency, with distributed beamforming enabled from the third frame onwards. For continuous communication, we would be beamforming in a given frame based on pilots sent two frames back. If the feedback link is the bottleneck, then the frame length T_f must be long enough to carry back the feedback corresponding to M_p pilot subcarriers on $L \geq N$ OFDM symbols, which amounts to $2M_pL$ bits using 2-bit feedback. For feedback of rate R_f, this corresponds to a frame length of $T_f = \frac{2M_pL}{R_f}$, and a channel coherence time of $T_c = 3T_f$. If the feedback link is not the bottleneck, then the minimum frame length can be set to $T_f = LT_{\text{OFDM}}$, where T_{OFDM} is the OFDM symbol length, which is governed by the channel delay spread and the overhead allowed for the cyclic prefix. We provide numerical values for our running example of a 20 MHz downlink over an EPA channel model at the end of this section.

We first discuss achievable performance on the downlink, and then consider the feedback link. In both cases, we use outage rates for a compact bottom-line characterization.

4.5.1 Downlink Performance

We assume that each node in the DBS cluster applies a phase correction on each subcarrier based on its channel estimate, and employs a uniform power distribution across subcarriers. Since the DBS nodes do not have information regarding the relative channel strengths across subcarriers or transmitters, more optimal power allocation methods

such as waterfilling are not possible. Even for a narrowband channel, using multiple transmitters for distributed beamforming provides spatial diversity, hence we derive a pessimistic estimate of outage spectral efficiency by ignoring frequency diversity and focusing on a single subcarrier at frequency f_k. The channel seen by node i is denoted as $H_i(f_k)$. Upon ideal phase compensation, the net channel seen at the receiver is given by $\|\mathbf{H}(f_k)\|_1 = \sum_{i=1}^{N} |H_i(f_k)|$, where $\mathbf{H}(f_k) = (H_1(f_k), ..., H_N(f_k))^T$ is the vector of channel gains corresponding to the N nodes in the DBS cluster. Modeling the channels $\{H_i(f_k)\}$ as zero mean complex Gaussian normalized as $E[|H_(f_k)|^2] = 1$, the effective channel amplitude gain $\|\mathbf{H}(f_k)\|_1$ is a sum of i.i.d. Rayleigh random variables, each with mean squared value of one.

Assuming that each transmitter applies power P to each subcarrier, the outage probability for a narrowband system operating at f_k is given by

$$\begin{aligned} p_{\text{out}}(R) &= \mathbb{P}\left\{ \log_2\left(1 + \frac{P\|\mathbf{H}(f_k)\|_1^2}{N_0}\right) < R \right\} \\ &= \mathbb{P}\left\{ \|\mathbf{H}(f_k)\|_1 < \sqrt{(2^R - 1)\frac{N_0}{P}} \right\} \end{aligned} \tag{4.11}$$

The ϵ-outage capacity C_ϵ is the maximum rate R such that $p_{\text{out}}(R)$ is less than ϵ.

Letting $F(\cdot)$ denote the CDF of $\|\mathbf{H}(f_k)\|_1$, we see that

$$C_\epsilon = \log_2\left(1 + \frac{P}{N_0} F^{-1}(\epsilon)^2\right) \tag{4.12}$$

Since $\|\mathbf{H}(f_k)\|_1 = \sum_{i=1}^{N} |H_i(f_k)|$ is a sum of i.i.d. random variables, we get insight, and a good approximation, by applying the central limit theorem. That is, we can approximate $\|\mathbf{H}(f_k)\|_1$ as Gaussian with mean $\mu = N\sqrt{\pi/4}$ and variance $\sigma^2 = N(1 - \pi/4)$. Using this

approximation in (4.12), we obtain that

$$C_\epsilon \approx \log_2\left(1+\frac{P}{N_0}\left(N\sqrt{\tfrac{\pi}{4}}-\sqrt{N\tfrac{(1-\pi)}{4}}Q^{-1}(\epsilon)\right)^2\right) \tag{4.13}$$

where $Q(\cdot)$ denotes the complementary CDF of a standard Gaussian random variable. This indicates that that the outage capacity shows a $\log N$ growth with the number of nodes, with $O(\sqrt{N})$ backoff within the argument of the logarithm in order to handle the tails.

The Gaussian approximation works well for moderately large N, including our running example of $N = 10$, and provides insight into the benefits of both spatial diversity and beamforming. We note, however, that for small N, the outage capacity approximation can be improved by using a small argument approximation to the CDF F of a sum of i.i.d. Rayleigh random variables [48], given by

$$\begin{aligned} F_{\mathrm{SAA}}(t\sqrt{N}) &\approx 1-e^{-\frac{t^2}{2b}}\sum_{k=0}^{N-1}\frac{(\frac{t^2}{2b})^k}{k!} \\ b &= \frac{\sigma^2}{N}\big[\prod_{i=1}^{N}(2i-1)\big]^{1/N} \end{aligned} \tag{4.14}$$

where $t = \frac{x}{\sqrt{N}}$ is a normalized argument for the CDF. This approximation, when used in (4.12), is excellent for small values of t which is the regime of interest for the outage probabilty ϵ.

We compare these approximations with simulations in the next section.

Numerical results

Figure 4.10 shows the ergodic capacity and the outage rate versus the number of transmitters at -5 dB SNR per node for a narrowband channel with ideal channel state information. The ergodic capacity and the 1% outage rate curves are obtained with Monte

Carlo simulations. The analytical outage capacity approximation for sum of Rayleigh random variables in (4.14) matches Monte Carlo simulations very well and the Gaussian aprroximation of the sum of Rayleigh random variables (4.13) is slightly pessimistic for the small number of nodes. The difference between ergodic capacity and outage rate diminishes as the number of nodes increases because the diversity gain provided by multiple nodes reduces the variance of the aggregate channel and, in turn, the variance of spectral efficiency. It can be observed that, with $N = 10$ nodes, the outage capacity of 3.5 bps/Hz can be obtained at -5 dB SNR per node.

Figure 4.11 shows Monte Carlo simulation results for outage capacity versus number of transmitters applied to the wideband setting (i.e., where the spectral efficiency is averaged over the signal bandwidth) with parameters in Table 4.2 at -5 dB average SNR. The ideal CSI curve shows the capacity when the channel is known to all nodes and perfect beamforming is applied over the entire frequency band. The DOST curve shows Monte Carlo simulation results with 2 bits of feedback per pilot subcarrier. The heavily quantized DOST algorithm provides significant gains in terms of capacity and is able to achieve outage rate of 3.1 bps/Hz using 10 nodes. Thus, even while operating at a per-node SNR of -5 dB, DOST can yield a data rate of about 50 Mbps over a 20 MHz band, after accounting for the overhead of reserving 1/6 of the subcarriers for pilots, under the assumption that we would like to be as reactive to channel time variations as possible and therefore insert comb type pilots into every OFDM symbol. For transmit power of 20 dBm (100 mW) per DBS node, isotropic antennas, and receiver noise figure of 6 dB, the attainable range using the Hata propagation model at 800 MHz carrier frequency with 30 m DBS node height and 1.5 m receiver height is about 6.6 km, allowing for a 5 dB implementation margin (we already account for fading in our formulation, hence we do not require excess link margin to accommodate it). The range that can be attained in the same setting for the same target data rate is 2.3 km for a single node and 4.2 km with

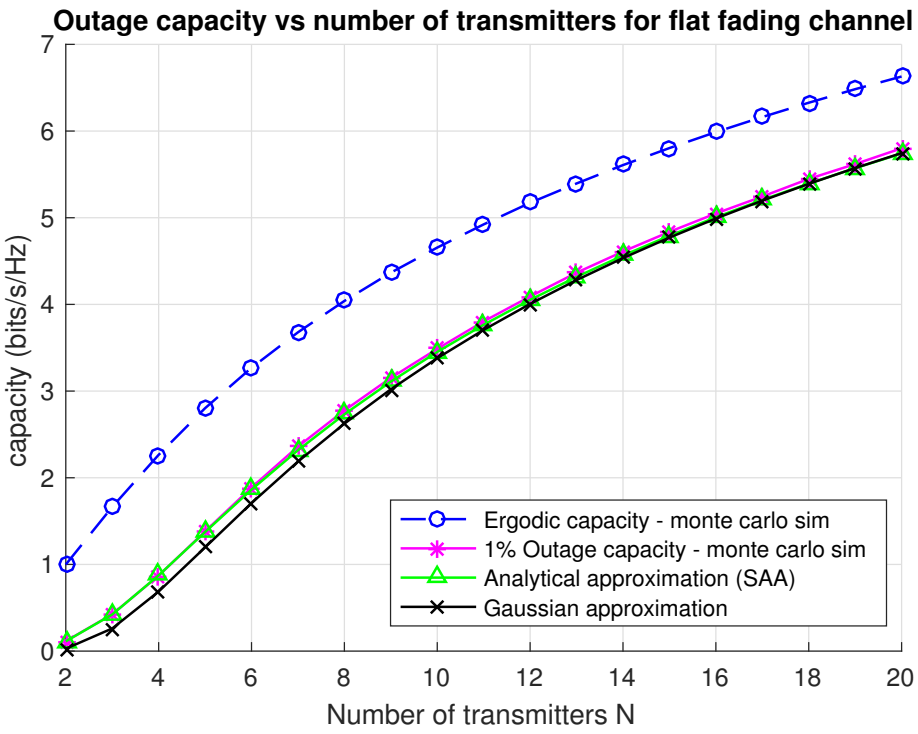

Figure 4.10: Ergodic capacity and 1% outage rates (b/s/Hz) versus number of nodes for narrowband flat fading channel at SNR = −5 dB

power pooling. As expected, the corresponding numbers at a lower carrier frequency of 200 MHz are better: 5 km for a single node, 9 km with power pooling, and 14.3 km with DOST.

4.5.2 Feedback link

While we do not consider detailed design of the feedback link, we provide insight into the impact of reception strategy by comparing three different options. The first and simplest approach is to designate a single node (e.g., one of the DBS nodes) as receiver for the feedback. In this case, the received SNR is very low (e.g., −5 dB for our running example, assuming that the emitted power from a DBS and user node are similar), and the feedback link becomes a significant bottleneck. A second approach is to attempt to

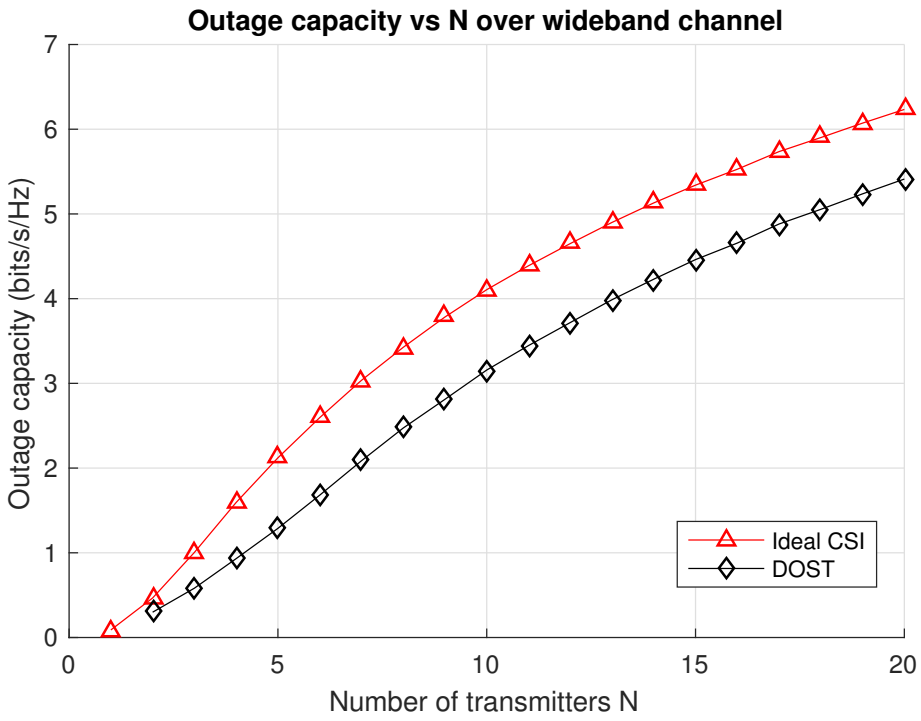

Figure 4.11: 1% outage rates (b/s/Hz) vs N for wideband channel at average SNR = −5 dB

decode the feedback packet at each DBS node separately, and to assume that successful decoding at any node will enable all other nodes to obtain the feedback via broadcast on a fast local area network (LAN). The third, and most complex, is distributed receive beamforming. Digitization and local transmission of the received signals at the N DBS nodes to a centralized processor requires that the LAN speed scale with N. It has been shown in [47] that much of the received beamforming gains (within 2 dB of ideal) can be obtained even if hard decisions are exchanged: this still requires LAN speed scaling with N, but at a smaller rate. Amplify-forward approaches for receive beamforming which sidestep such local communication by enabling on-air combining have also been proposed and demonstrated [33]. We therefore consider ideal receive beamforming as providing a performance benchmark for the feedback channel that may be attainable with sufficient engineering effort.

The bandwidth on the feedback link may be different (typically smaller, since multiple user nodes may be sending feedback to the DBS) from that on the downlink. We average the spectral efficiency across this bandwidth when determining outage rates.

In the first approach, for a discrete set of M_u subcarriers, the spectral efficiency at a given DBS node, say node k, can be calculated as

$$I_k = \frac{1}{M_u} \sum_{i=1}^{M_u} \log_2(1 + \text{SNR}|H_k(f_i)|^2) \tag{4.15}$$

where $H_k(f_i)$ is the uplink channel on the ith subcarrier for the kth DBS node. We can now define the ϵ-outage rate R_u as usual

$$P(I_k < R_1) = \epsilon. \tag{4.16}$$

For the second approach, outage occurs if all of the DBS nodes are unable to decode the feedback packet:

$$P\left(max(I_1, I_2, ..., I_N) < R_2\right) = \epsilon. \tag{4.17}$$

Assuming that the channel realizations for the different nodes are i.i.d., we infer that the random variables $I_1, ..., I_N$ are i.i.d., so that $P\left(max(I_1, I_2, ..., I_N) < R_2\right) = \left(P(I_1 < R_2)\right)^N$. Thus, we obtain that the outage rate satisfies

$$P\left(I_1 < R_2\right) = \epsilon^{\frac{1}{N}}. \tag{4.18}$$

which allows the individual outage probability at any DBS node to be much higher. We have checked via simulations that (4.17) and (4.18) yield the same results for our channels, which are obtained by independent draws from the EPA model.

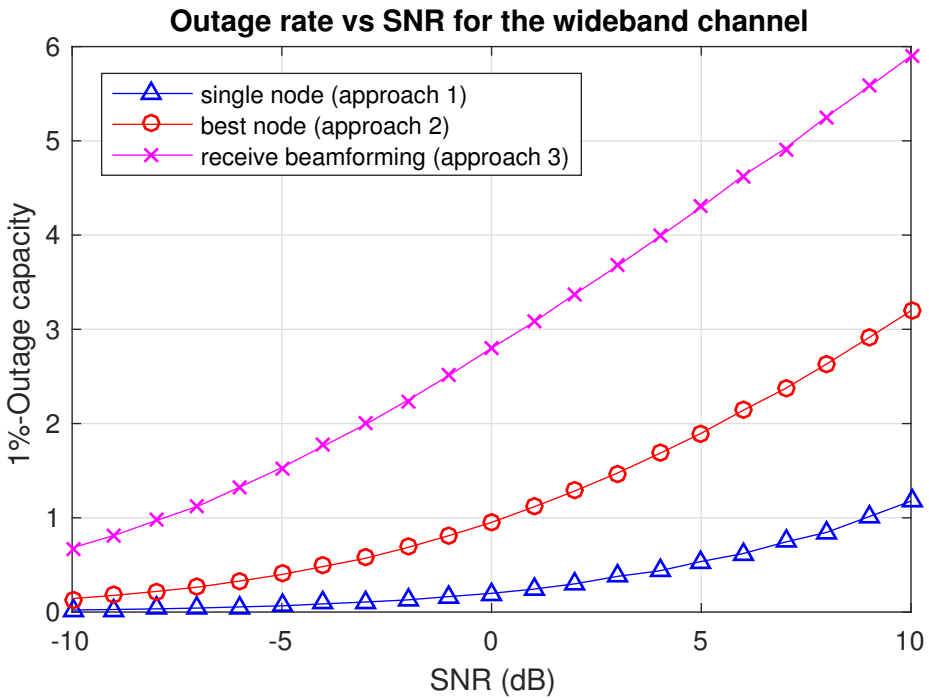

Figure 4.12: 1% outage rates vs per node SNR for wideband channels using 10% of the 20 MHz uplink bandwidth with single node, best node and ideal receive beamforming with using $N = 10$ nodes

For the third approach (receive beamforming), the spectral efficiency is given by

$$I_{\text{beam}} = \frac{1}{M_u} \sum_{i=1}^{M_u} \log_2 \left(1 + \text{SNR}(\sum_{k=1}^{N} |H_k(f_i)|^2) \right) \tag{4.19}$$

and the outage rate satisfies

$$P\left(I_{\text{beam}} < R_3\right) = \epsilon. \tag{4.20}$$

Figure 4.12 shows the outage rates for the three approaches computed over a $W_{\text{fb}} = 2$ MHz bandwidth for the feedback link. For a per-node SNR of -5dB, the outage rates are given by $R_1 = 0.066$, $R_2 = 0.4$, and $R_3 = 1.5$ bps/Hz. These translate to feedback data rates R_f of 132 Kbps, 0.8 Mbps, and 3 Mbps, respectively. Assuming that the feedback

link is the bottleneck, and that $L = N$, we compute the corresponding frame lengths as

$$T_f = \frac{2NM_p}{R_f} \tag{4.21}$$

The minimum channel coherence times $T_c = 3T_f$ that can be supported using the three approaches are given by 90, 15 and 3.9 ms respectively.

We conclude that, even though the SNR on the feedback link is so low, the first approach is adequate for quasi-static links typical of rural broadband. However, if more sophisticated strategies such as the second or third approaches are employed, the DBS concept can be used to support moderate mobility.

Chapter 5

Distributed 911: RF Source Seeking as a Building Block

5.1 Introduction

The D911 concept system is based on search-and-rescue or other emergency applications in which a cluster of cooperating low-cost and low-power devices try to communicate with a distant mobile emergency vehicle which a single device may not be able to reach. Incoherent power pooling gain or beamforming gain from pre-synchronization of multiple nodes (as done in prototypes such as could potentially be used for range extension to broadcast a periodic pilot signal to draw mobile emergency vehicle to the vicinity of a cluster of nodes.

As an initial step to realize a D911 concept system, we consider a scenario where an unmanned aerial vehicle (UAV) seeks to approach a single RF source, starting from an initially large distance. The UAV is equipped with a single omnidirectional antenna, and does not rely on GPS or on being able to decode messages from the emitter. The source may be surrounded by local scatterers. We propose an approach in which the UAV

adapts its trajectory towards the emitter using frequency measurements on the received beacon. In an ideal line of sight (LoS) environment, a single omni-directional antenna can extract the angle of the arrival θ between the velocity vector of the mobile node and LoS to the source by measuring the Doppler frequency $f_d = \frac{v\cos\theta}{c} f_c$, where v is the velocity and c is the speed of light. Thus, a natural approach is for the UAV to follow the trajectory that maximizes the Doppler shift (which corresponds to $\theta = 0$). However, translating this intuition into a working approach requires that we address the following technical challenges:

1) The scattering environment around the source causes multipath fading, resulting in large spatial variations of the received signal power. This can often lead to errors in frequency measurements, especially at the low received signal-to-noise ratio (SNR) obtained at large distances.

2) The local oscillators at the emitter and UAV are not synchronized, and drift over time. Thus, the frequency measurements made by the UAV are a sum of the Doppler shift and a slowly drifting carrier frequency offset.

3) Even in ideal LoS settings, Doppler estimates have direction ambiguity: if the trajectory makes an angle θ with the LoS, then the Doppler shift is proportional to $\cos\theta$, and cannot therefore enable us to distinguish between $+\theta$ and $-\theta$.

4) Any trajectory adaptation done by the UAV should be feasible, avoiding sharp direction changes.

The main contribution of this chapter is to show that we can indeed overcome the preceding difficulties to obtain a scheme that reaches the vicinity of the emitter, with net distance traversed being only a small fraction (of the order of 10%) larger than the initial LoS distance between the UAV and the emitter. We consider a small UAV that flies at around 100 m altitude, listening to a beacon in commercial frequency bands (the carrier frequency is set to 2 GHz in our numerical examples). The initial distance between

the UAV and the source is of the order of 5 km. In our proposed approach, the UAV obtains an initial trajectory estimate by finding the direction of maximum Doppler when executing a circular motion. Subsequently, it employs feedback control to continuously adapt its trajectory, using the change in measured frequency offset as it executes designed piecewise linear deviations in bearing from the nominal trajectory.

The proposed approach performs significantly better than RF source following using received signal strength (RSS) measurements [49]. While RSS measurements are simpler to make and do not require coherent processing at the receiver, the sensitivity of RSS change as a function of range to the emitter is small even in ideal settings, since it is proportional to the inverse square of the range. In addition, local scatterers around the emitter lead to slow, and deep, spatial variations in RSS due to fading. The approach in [49] employs the observation that the rate of change of RSS due to fading is minimum in the LoS direction, along with a random walk inspired by bacterial chemotaxis. For a setting similar to ours, the RSS-based scheme requires the UAV to traverse a distance that is about three times larger than the shortest path between the initial UAV location and the emitter. Furthermore, the trajectories employed in [49], both for initialization and for the random walk, are non-smooth and difficult to execute.

RSS measurements are more effective if supplemented with *directional* information. A rotating UAV was employed in [50], with the angle of arrival to the emitter estimated as the direction of maximum RSS. This approach is not applicable to fixed wing UAVs with omnidirectional antennas as considered here.

While we consider the problem of *approaching* the emitter, there is a significant literature on *localizing* the emitter using a mobile platform [51, 52] or multiple mobile platforms [53, 54]. Particle filter based algorithms for tracking the posterior distribution of the emitter are investigated in [55, 56]. In addition to having a different design goal from ours, it is worth noting that these approaches require that the mobile platform

always knows its own absolute location, say using GPS. Our problem formulation requires the UAV to track changes in its own bearing, but does not require that it know its absolute location, and hence is applicable even in GPS-denied environments.

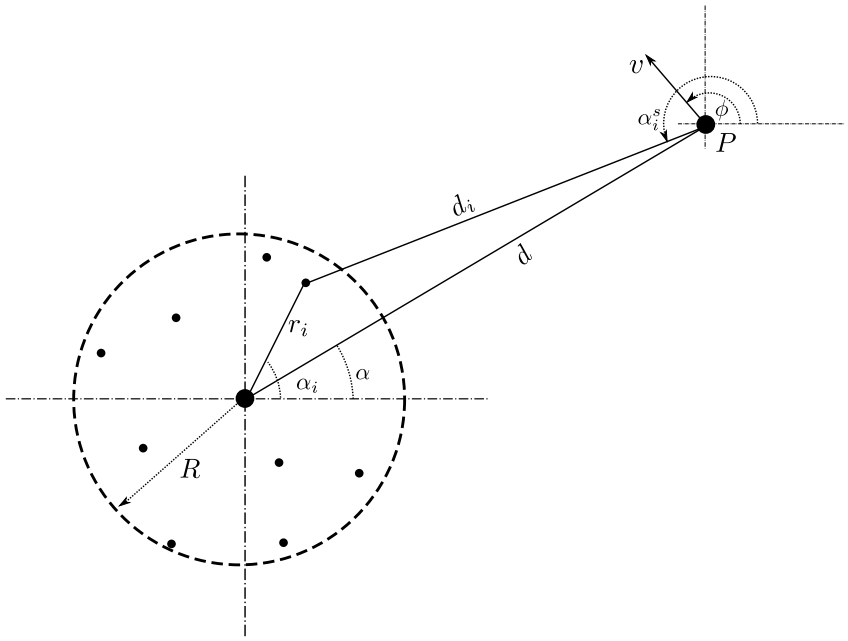

Figure 5.1: System model in 2D, scatterers on a disk around the source

5.2 Channel Model

The problem of drawing the UAV to the emitter location is three-dimensional, but we restrict the problem to two dimensions for simplicity. As shown in Figure 5.1, the source is located at the the origin of the 2D plane, and is surrounded by L local scatterers. The UAV coordinates at any given time are denoted by $p = (x, y)$ with velocity components $v_x = v\cos(\phi)$ and $v_y = v\sin(\phi)$. The distance between the mobile receiver and the source is d. The scatterers are inside an annulus with outer radius R and inner radius R_{in}, and the angles $\{\alpha_i\}$ are uniformly distributed between $-\pi$ and π for each scatterer.

We consider a narrowband flat fading channel at carrier frequency f_c, and assume

that the receiver will compute its estimates based on known pilot signals transmitted by the source. The complex baseband channel seen by the mobile node can be expressed as the sum of LoS and scattered components and can be written as

$$\begin{aligned} h(t) =& \sqrt{\frac{K\sigma_h^2}{K+1}} e^{j(2\pi f_{d,max}\cos(\alpha-\phi)t+2\pi f_o(t)t+\psi_0)} + \\ & \sqrt{\frac{\sigma_h^2}{K+1}} \sum_{i=1}^{L} e^{j(2\pi f_{d,max}\cos(\alpha_i^s-\phi)t+2\pi f_o(t)t+\psi_i)} + n(t) \end{aligned} \tag{5.1}$$

where K is the ratio of power between the direct path and the scattered paths, $f_{d,max} = \frac{vf_c}{c}$ is the maximum Doppler frequency, $f_o(t)$ is the carrier frequency offset drifting over time, ψ_0 and ψ_i are the phase of LoS and scattered signal components respectively, σ_h^2 is the received signal power and $n(t)$ represents the additive noise at the receiver with the variance σ_n^2.

The received signal strength σ_h^2 is governed by the distance between source and mobile receiver d, along with spatial variations due to multipath fading. The effect of Doppler frequency on the received signal profile is negligible at these low speeds since $f_c \gg f_{d,max}$. We model the received signal strength by modeling the electric field at the mobile node at a point P in polar coordinates (d, α) as[49]:

$$EF(d,\alpha) = \frac{e^{-j\beta d}}{d} + \sum_{i=1}^{L} \frac{\Gamma_i e^{-j\beta(d_i+r_i)}}{d_i + r_i} \tag{5.2}$$

where $\beta = \frac{2\pi}{\lambda}$ and λ is the wavelength, $d_i + r_i$ is the total distance of the path that goes from the source to receiver through ith scatterer and Γ_i is the reflection coefficient for the ith scatterer [32].

Frequency estimation accuracy in a flat fading channel, assuming all paths have the same frequency offset, is proportional to the received SNR [57]. This assumption is a

good approximation for our model when $d \gg R$. We use low-complexity single tone frequency estimation [58], selecting the maximum frequency over the DFT grid, and then interpolating using a quadratic fit. As the UAV gets closer to the source, each path sees a different frequency offset due to the difference in the reflection angles, and the frequency estimate degrades. Estimation accuracy in this region could potentially be further improved with frequency estimates derived from second order statistics [59], or by employing super-resolution techniques [60]. However, at shorter ranges, more sophisticated frequency estimation should be coupled with more detailed anisotropic reflection models, hence we leave this as an interesting topic for future work (e.g., on how to track a moving emitter in urban canyons).

5.3 The Algorithm for Source Seeking

In this section, we describe and justify the strategy for planning the UAV trajectory by using frequency measurements and show that the proposed algorithm will converge to the true source direction with no prior information on the source location. The purpose is to draw UAV to the vicinity of the emitter as quickly as possible. We set $d_v \ll d$ as the required distance between UAV and the source at which we declare the tracking process successful. We assume constant speed through the trajectory of the UAV and use a feasible trajectory for the motion of UAV. The goal is to minimize flight time.

We assume prior knowledge of the emitted signal carrier frequency f_c, but not of the carrier frequency offset f_o, which also drifts over time. The pilot beacon for a given frequency measurement contains N symbols, with symbol period T_s, so that the measurement interval for frequency estimation is $T = NT_s$. The pilot beacons are repeated with the period of T_{slot}.

For the nth received beacon, frequency measurements are obtained by applying FFT

to the N complex baseband samples of (5.1), and the peak frequency $\hat{\omega}_i$ $i \in 1, \cdots, N_{FFT}$ is refined by using a quadratic interpolation with adjacent samples:

$$\tilde{\omega}_n = \hat{\omega}_i + \frac{\hat{\omega}_{i-1} - \hat{\omega}_{i+1}}{2(\hat{\omega}_{i-1} + \hat{\omega}_{i+1} - 2\hat{\omega}_i)} \frac{2\pi}{T_s N_{FFT}} \tag{5.3}$$

Thus, we obtain a noisy estimate of the sum of carrier frequency offset, Doppler frequency and the frequency drift. We model this, together with the bearing angle measured by the UAV sensors, as

$$\begin{aligned} \tilde{\omega}_n &= \omega_n + n_{\omega,n} \\ \tilde{\phi}_n &= \phi_n + n_{\phi,n}. \end{aligned} \tag{5.4}$$

where $n_{\omega,n}$ and $n_{\phi,n}$ are frequency measurement and bearing measurement noises, modeled as zero mean independent Gaussian random variables with variances $\sigma^2_{\omega,n}$ and $\sigma^2_{\phi,n}$, respectively. The bearing measurement error variance $\sigma^2_{\phi,n}$ is assumed to be constant throughout the flight. However, the frequency measurement error variance $\sigma^2_{\omega,n}$ can vary: it increases as RSS drops during fades, and as Doppler spread increases as the UAV approaches the emitter.

While we do not model the UAV dynamics, we will restrict the algorithm described in the next section to use trimming trajectories, which have the desirable property that the tracking error dynamics and kinematics about is time invariant and for which there are well-developed trajectory tracking controllers [61, 62, 63]. The orientation tracking error about the desired trimming trajectory is included in error parameter $n_{\phi,n}$.

5.3.1 Trajectory adaptation

The source tracking algorithm can be divided into two stages, discussed in more detail below. In the first stage, the UAV gets a rough estimate of the direction of the source by doing a circular motion. This stage is actually optional, and can be removed at the expense of some inefficiency in flight time. The second stage involves piecewise linear trajectories with perturbations of bearing which provide a feedback signal in terms of change in Doppler to drive continuous trajectory corrections.

Stage 1 - Circular motion for initial trajectory estimate

The UAV picks a random point at a distance R_c and follows a circular trajectory, as shown in Figure 5.2, saving the frequency measurements $\tilde{\omega}_n$ with corresponding bearing measurements $\tilde{\phi}_n$. The largest frequency measurement corresponds to the maximum Doppler $f_{d,max}$ and bearing angle that corresponds to the desired direction is approximately $\pi + \alpha$ in an ideal setting. The smallest frequency measurements corresponds to the $-f_{d,max}$ at the direction of α.

The SNR is low when UAV is very distant, and multipath fading may occasionally result in large outliers in the frequency measurements $\tilde{\omega}_n$. We apply outlier rejection to the frequency measurements as

$$\breve{\omega}_n = \begin{cases} \tilde{\omega}_n, & |\tilde{\omega}_n - \tilde{\omega}_{n-1}| < 4\pi \frac{v f_c}{c} \\ \tilde{\omega}_{n-1}, & \text{otherwise} \end{cases} \tag{5.5}$$

and apply a moving average filter with length 15 T_{slot}. Then, the initial direction for

UAV is determined by finding the direction of maximum frequency estimate as follows

$$i = \underset{n}{\operatorname{argmax}}\, \breve{\omega}_n$$
$$\theta_0 = \tilde{\phi}_i. \tag{5.6}$$

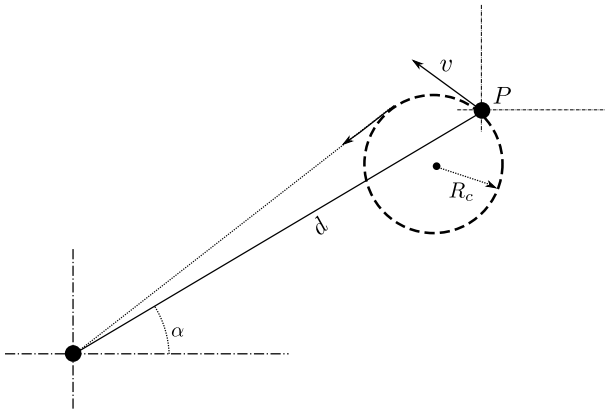

Figure 5.2: Initial circular motion of the UAV

Stage 2 - Continuous updates

In this stage, the UAV derives information for feedback control of its trajectory in discrete time steps spanning $2MT_{slot}$ for each step. If the estimated direction towards the emitter is θ_k from the previous direction, the UAV moves in the direction $\theta_k + \delta_k$ for a time interval with length MT_{slot}, yielding frequency measurements $\{\breve{\omega}_m, m = 1, ..., M\}$, and then in the direction $\theta_k - \delta_k$ for the same duration, yielding measurements $\{\breve{\omega}_m, m = M+1, ..., 2M\}$. The difference between these two sets of frequency measurements is used to update θ_k, as follows:

$$\theta_{k+1} = \theta_k + \frac{1}{M}\Big(\sum_{m=1}^{M} \breve{\omega}_m - \sum_{m=M+1}^{2M} \breve{\omega}_m\Big)\frac{\delta_k}{2\pi f_{d,max}}. \tag{5.7}$$

Taking the difference in this fashion allows significant reduction of the effect of carrier frequency offset and drift, which vary slowly relative to the iteration step duration $2MT_{slot}$. Additional robustness against measurement noise can be obtained by increasing the perturbation δ_k, at the cost of increased travel distance.

The initial estimate θ_0 from stage 1 helps improve the convergence time of stage 2, but the latter also works with a random initialization.

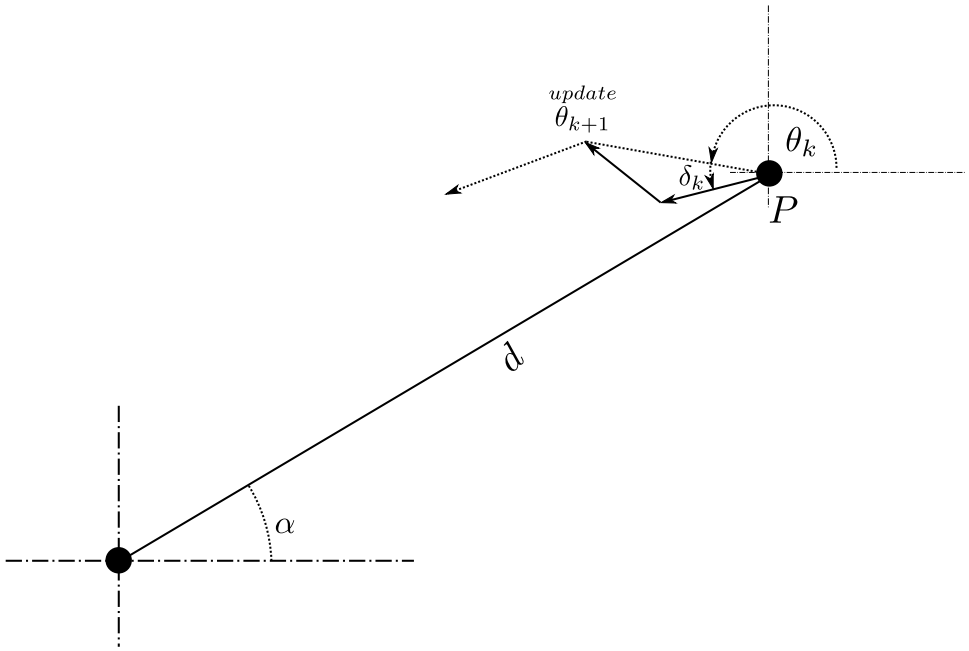

Figure 5.3: Updating the direction of the UAV by perturbing the direction with $\pm\delta_k$

5.4 Analysis

We provide analytical insight for the convergence of the proposed algorithm in stage 2 by showing that the error term for the estimation of true direction $\theta_k^* = \pi + \alpha_k$ decreases over time. Straightforward trigonometry shows that the update step in (5.7) with a

constant $\delta_k = \delta$ can be written as

$$\begin{aligned}\theta_{k+1} &= \theta_k + (\cos(\theta_k - \theta_k^* + \delta) - \cos(\theta_k - \theta_k^* - \delta))\,\delta \\ &= \theta_k - 2\sin(\theta_k - \theta_k^*) sin(\delta)\delta.\end{aligned} \tag{5.8}$$

Let the error term $\tilde{\theta}_k = \theta_k - \theta_k^*$. For $d \gg ||p_{k+1} - p_k||_2$ (range much larger than the distance between consecutive iterations), we have $\theta_k^* \approx \theta_{k+1}^*$, which enables us to write the error term as

$$\tilde{\theta}_{k+1} = \tilde{\theta}_k - 2\sin(\tilde{\theta}_k) sin(\delta)\delta \approx \tilde{\theta}_k(1 - 2\delta^2), \tag{5.9}$$

Thus, the estimation error decreases exponentially, by a factor of $1 - 2\delta^2$ over each iteration. Increasing δ improves the convergence time, but comes at the cost of additional flight time and sharper turns.

Picking $\tilde{\theta}_k^2$ as a Lyapunov function, we conclude that it's change in one time-step is given by:

$$\tilde{\theta}_{k+1}^2 - \tilde{\theta}_k^2 \leq -4\alpha \sin\tilde{\theta}_k(\tilde{\theta}_k - \alpha \sin\tilde{\theta}_k)$$

where $\alpha = \delta \sin\delta$. This shows that $\tilde{\theta}_k^2$ is a strictly decreasing function as long as $\sin\tilde{\theta}_k(\tilde{\theta}_k - \alpha \sin\tilde{\theta}_k)$ remains strictly positive, which is case for every $\alpha < 1$. This provides a wide range of choices for δ.

5.5 Simulation Results

The simulation parameters are given in Table 5.1. We apply $N_{FFT} = 4096$ point FFT to $N = 1000$ data chunks in every $T_{slot} = 50ms$ for frequency estimation. The average received SNR at the initial distance of 5 km is set to 0 dB. Figure 5.4 shows an example UAV trajectory. Figure 5.5 shows the estimated frequency in the presence of

multipath, CFO and frequency drift for that particular trajectory. Figure 5.5 also shows the received signal power profile through the trajectory and the spatial variations at the received power. We observe that the frequency estimation error increases as the UAV gets closer to the source due to increased Doppler spread.

Parameters	
Parameter Symbol	Value
d	5000 m
R	200 m
R_{in}	100 m
f_c	2 GHz
v	10 m/s
σ_n^2	-70 dB
T_{slot}	50 ms
T	10 ms
T_s	10 us
N_{FFT}	4096
δ	10^o
d_v	$200m$
M	20

Table 5.1: Simulation parameters

Figure 5.6 shows the histogram of the total distance traveled with Monte Carlo simulations of 1000 runs for the same scenario. The average distance traveled is 5.5 km, which is 1.15 times the shortest path to get within the desired distance of the target. This significantly outperforms the RSS based algorithm [49], for which the average distance traveled is about 3 times of the shortest path. The proposed algorithm works even if we discard stage 1 and use a random initial direction. Figure 5.7 shows the histogram of the total distance traveled with Monte Carlo simulations of 1000 runs with only Stage 2 of the algorithm. The average tracking distance is now 6 km, which is 1.25 times the shortest path approach.

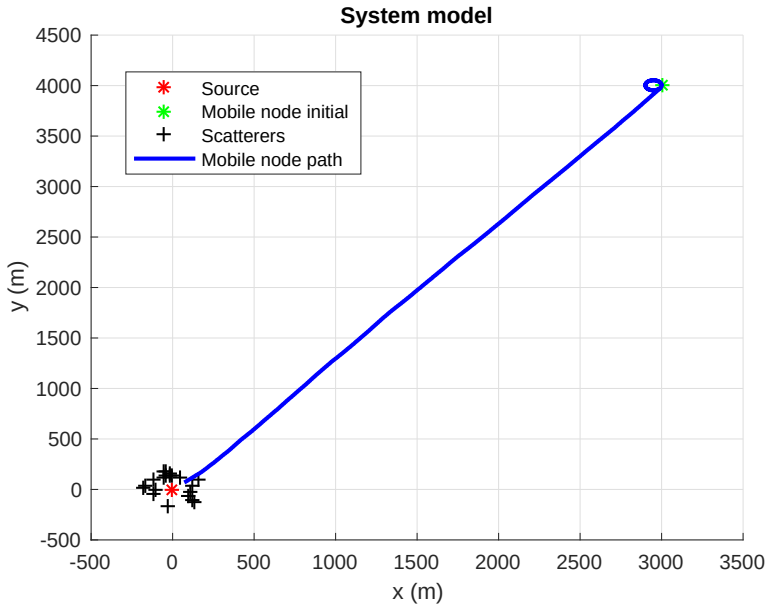

Figure 5.4: An example trajectory with the 0 dB average SNR with the initial distance of 5 km

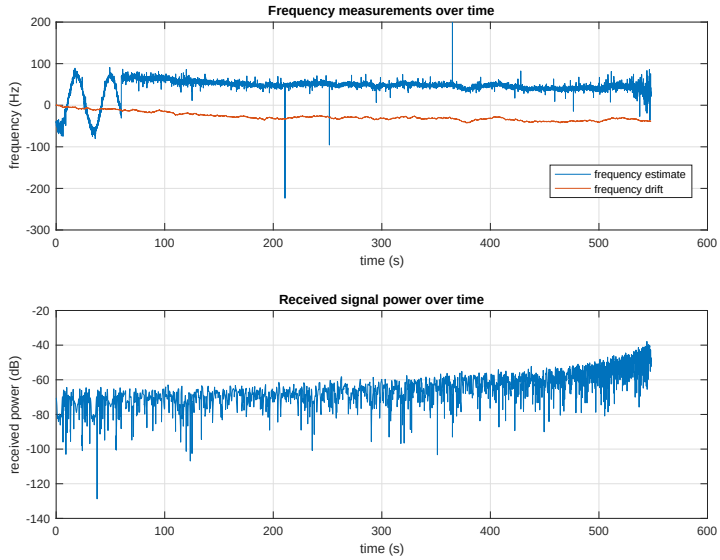

Figure 5.5: Frequency measurements and the received signal strength trough the route in Figure 5.4

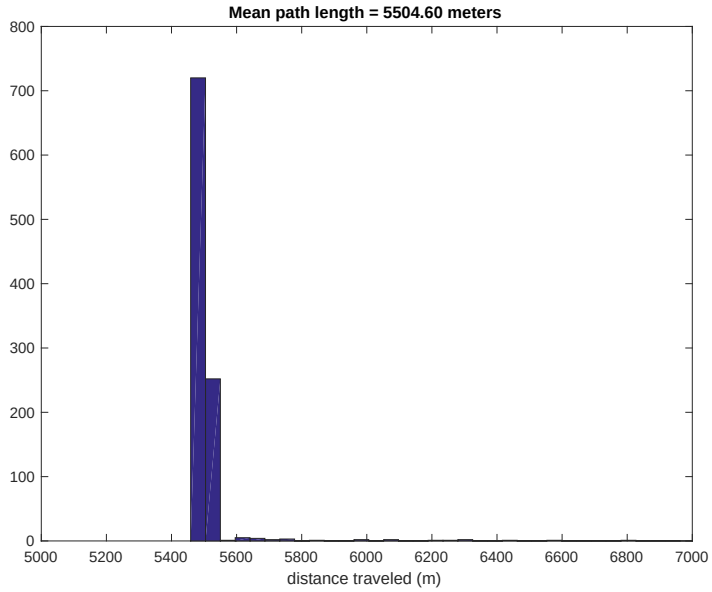

Figure 5.6: Histogram of the total distance traveled to get the 200m vicinity of the source (mean ~ 5.5km)

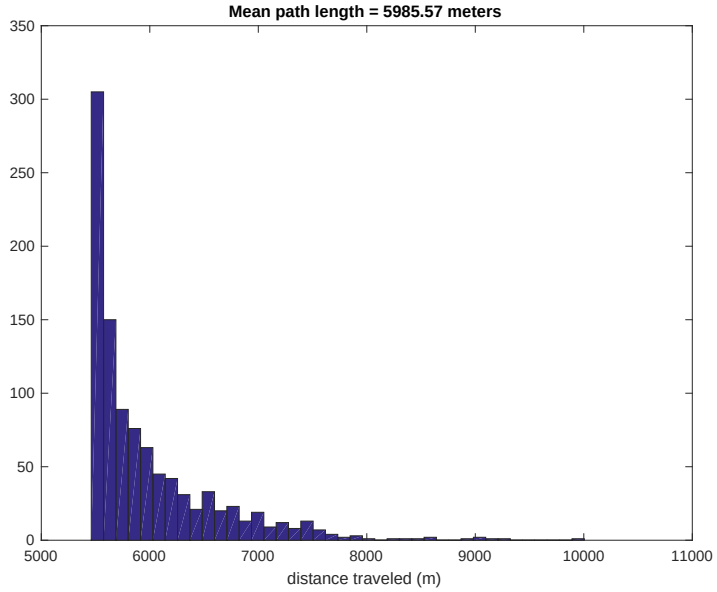

Figure 5.7: Histogram of the total distance traveled to get the 200m vicinity of the source using random initialization, without using stage 1 (mean ~ 6km)

Chapter 6

Conclusion and Future Work

6.1 Algorithms and Protocols

We investigated the extension of narrowband distributed beamforming algorithms to wideband systems in high-SNR scenarios. Applying the one bit feedback algorithm to each subcarrier independently causes phase discontinuities among subcarriers. We proposed an algorithm which uses a second feedback bit to ensure phase continuity. We applied the proposed 2-bit feedback algorithm to a subset of subcarriers in order to keep feedback overhead low, using linear interpolation for the remaining subcarriers. The proposed approach enables the target node to be oblivious to the number of virtual antenna array nodes in a wideband setting. Thus, classical OFDM channel estimation algorithms via demodulation reference signals can be used at the target node, with the virtual antenna array acting as a single node. Simulation results using a 2-bit feedback algorithm showed that the gain beyond power pooling is limited in low-SNR scenarios due to the vulnerability of the one bit feedback algorithm to the noise.

Motivated by these findings, we analyzed the one bit feedback algorithm in noisy scenarios. We showed that the virtual antenna array size cannot be scaled indefinitely

using the one bit feedback algorithm. Only a fraction of ideal beamforming gain can be attained as the per-node SNR gets small. This is because the progress of RSS over a step of the algorithm scales in the same manner as receiver noise, as shown by the covariance computations under our joint Gaussian approximations.

We proposed the DOST algorithm to overcome the noise bottleneck in the previous beamforming algorithms. The training using the incoherent power pooling gain boosts the effective SNR, which provides the flexibility to scale down SNR per node, as long as we are willing to increase the length of the training period correspondingly. The DOST algorithm can work with quantization as drastic as one bit per real and imaginary dimension, hence the feedback overhead is similar to those of other distributed beamforming algorithms. We also showed that the DOST algorithm can be extended to wideband systems using either linear interpolation across subset of subcarriers or sparse time domain reconstruction.

6.2 Concept Systems

The DBS concept system using the DOST algorithm is a promising approach to provide broadband access to remote areas by scaling the array size of the distributed MIMO on large carrier wavelengths. We compactly characterized DBS performance with outage capacity analysis. We showed that a significant range extension (e.g., from 2 km to 6 km by using 10 nodes at 800MHz in a rural setting), can be achieved. We observed that the feedback link can become a bottleneck since propagation loss due to range extension also decreases the feedback link SNR. We showed that it is possible to support DBS system in relatively slow varying links (e.g., with coherence time of the order of 100 ms) with simple uplink reception techniques. Receive beamforming can be employed to overcome the low SNR on the feedback link. Investigation of distributed reception

techniques and simultaneous distributed transmit and receive beamforming strategies are interesting directions for future research. The gains promised by our design and analysis of the DBS concept system motivate efforts to prototype and experimentally demonstrate range extension.

As an initial step towards a distributed 911 concept system, we proposed a trajectory planning algorithm for RF source seeking problem by using frequency and heading measurements. The proposed algorithm continually corrects the heading direction of the UAV using consecutive frequency measurements, which reduce the uncertainty due to carrier frequency offset and drift. We showed that the UAV converges to the correct direction towards the RF source. We showed via simulations that the flight time is significantly reduced in our algorithm compared to those of prior RSS-based RF source seeking algorithms. There are several interesting directions for future work. First, the algorithm should be further analyzed in more complicated channel models (e.g., if the LoS is blocked, the UAV may follow a strong reflected path until it sees a LoS path again). Second, super-resolution frequency estimation algorithms can be used to distinguish paths and corresponding Doppler frequency in high Doppler spread scenarios. Third, more detailed accounting of UAV dynamics and fusion of frequency measurements with other information sources cab be possible future directions for RF source seeking.

Bibliography

[1] R. Mudumbai, D. R. Brown, U. Madhow, and H. V. Poor, *Distributed transmit beamforming: challenges and recent progress*, *IEEE Communications Magazine* **47** (2009), no. 2 102–110.

[2] S. Jayaprakasam, S. K. A. Rahim, and C. Y. Leow, *Distributed and collaborative beamforming in wireless sensor networks: Classifications, trends, and research directions*, *IEEE Communications Surveys & Tutorials* **19** (2017), no. 4 2092–2116.

[3] R. Mudumbai, J. Hespanha, U. Madhow, and G. Barriac, *Scalable feedback control for distributed beamforming in sensor networks*, in *Proceedings. International Symposium on Information Theory, 2005. ISIT 2005.*, pp. 137–141, IEEE, 2005.

[4] R. Mudumbai, G. Barriac, and U. Madhow, *On the feasibility of distributed beamforming in wireless networks*, *Wireless Communications, IEEE Transactions on* **6** (2007), no. 5 1754–1763.

[5] R. Mudumbai, J. Hespanha, U. Madhow, and G. Barriac, *Distributed transmit beamforming using feedback control*, *Information Theory, IEEE Transactions on* **56** (2010), no. 1 411–426.

[6] R. Mudumbai, B. Wild, U. Madhow, and K. Ramchandran, *Distributed beamforming using 1 bit feedback: from concept to realization*, in *Proceedings of the 44th Allerton conference on communication, control and computation*, pp. 1020–1027, 2006.

[7] F. Quitin, U. Madhow, M. M. U. Rahman, and R. Mudumbai, *Demonstrating distributed transmit beamforming with software-defined radios*, in *World of Wireless, Mobile and Multimedia Networks (WoWMoM), 2012 IEEE International Symposium on a*, pp. 1–3, IEEE, 2012.

[8] F. Quitin, M. M. U. Rahman, R. Mudumbai, and U. Madhow, *A scalable architecture for distributed transmit beamforming with commodity radios: Design and proof of concept*, *IEEE Transactions on Wireless Communications* **12** (2013), no. 3 1418–1428.

[9] F. Quitin, M. M. U. Rahman, R. Mudumbai, and U. Madhow, *Distributed beamforming with software-defined radios: frequency synchronization and digital feedback*, in *Global Communications Conference (GLOBECOM), 2012 IEEE*, pp. 4787–4792, IEEE, 2012.

[10] F. Quitin, A. Irish, and U. Madhow, *Distributed receive beamforming: A scalable architecture and its proof of concept*, in *Vehicular Technology Conference (VTC Spring), 2013 IEEE 77th*, pp. 1–5, IEEE, 2013.

[11] S. Song, J. S. Thompson, P.-J. Chung, and P. M. Grant, *Improving the one-bit feedback algorithm for distributed beamforming*, in *2010 IEEE Wireless Communication and Networking Conference*, pp. 1–6, IEEE, 2010.

[12] I. Thibault, G. E. Corazza, and L. Deambrogio, *Random, deterministic, and hybrid algorithms for distributed beamforming*, in *2010 5th Advanced Satellite Multimedia Systems Conference and the 11th Signal Processing for Space Communications Workshop*, pp. 221–225, IEEE, 2010.

[13] N. Xie, K. Xu, and J. Chen, *Exploiting cumulative positive feedback information for one-bit feedback synchronization algorithm*, *IEEE Transactions on Vehicular Technology* (2018).

[14] M. F. Gencel, M. E. Rasekh, and U. Madhow, *Scaling wideband distributed transmit beamforming via aggregate feedback*, in *Communications (ICC), 2015 IEEE International Conference on*, pp. 2356–2362, IEEE, 2015.

[15] M. F. Gencel, M. E. Rasekh, and U. Madhow, *Distributed transmit beamforming with one bit feedback revisited: How noise limits scaling*, in *Information Theory (ISIT), 2015 IEEE International Symposium on*, pp. 2041–2045, IEEE, 2015.

[16] M. F. Gencel, M. E. Rasekh, and U. Madhow, *Noise-resilient scaling for wideband distributed beamforming*, in *Signals, Systems and Computers, 2015 49th Asilomar Conference on*, pp. 276–280, IEEE, 2015.

[17] D. R. Brown III and H. V. Poor, *Time-slotted round-trip carrier synchronization for distributed beamforming*, *IEEE Transactions on Signal Processing* **56** (2008), no. 11 5630–5643.

[18] R. D. Preuss and D. R. Brown III, *Two-way synchronization for coordinated multicell retrodirective downlink beamforming*, *IEEE Transactions on Signal Processing* **59** (2011), no. 11 5415–5427.

[19] T. P. Bidigare, U. Madhow, D. R. Brown, R. Mudumbai, A. Kumar, B. Peiffer, and S. Dasgupta, *Wideband distributed transmit beamforming using channel reciprocity and relative calibration*, in *Signals, Systems and Computers, 2015 49th Asilomar Conference on*, pp. 271–275, IEEE, 2015.

[20] B. Peiffer, R. Mudumbai, A. Kruger, A. Kumar, and S. Dasgupta, *Experimental demonstration of a distributed antenna array pre-synchronized for retrodirective transmission*, in *Information Science and Systems (CISS), 2016 Annual Conference on*, pp. 460–465, IEEE, 2016.

[21] B. Peiffer, R. Mudumbai, S. Goguri, A. Kruger, and S. Dasgupta, *Experimental demonstration of retrodirective beamforming from a fully wireless distributed array*, in *Military Communications Conference, MILCOM 2016-2016 IEEE*, pp. 442–447, IEEE, 2016.

[22] E. Hamed, H. Rahul, M. A. Abdelghany, and D. Katabi, *Real-time distributed mimo systems*, in *Proceedings of the 2016 conference on ACM SIGCOMM 2016 Conference*, pp. 412–425, ACM, 2016.

[23] H. V. Balan, R. Rogalin, A. Michaloliakos, K. Psounis, and G. Caire, *Airsync: Enabling distributed multiuser mimo with full spatial multiplexing*, *IEEE/ACM Transactions on Networking (TON)* **21** (2013), no. 6 1681–1695.

[24] R. Irmer, H. Droste, P. Marsch, M. Grieger, G. Fettweis, S. Brueck, H.-P. Mayer, L. Thiele, and V. Jungnickel, *Coordinated multipoint: Concepts, performance, and field trial results*, *Communications Magazine, IEEE* **49** (2011), no. 2 102–111.

[25] A. Forenza, S. Perlman, F. Saibi, M. Di Dio, R. van der Laan, and G. Caire, *Achieving large multiplexing gain in distributed antenna systems via cooperation with pcell technology*, in *Signals, Systems and Computers, 2015 49th Asilomar Conference on*, pp. 286–293, IEEE, 2015.

[26] P. Harris, S. Zang, A. Nix, M. Beach, S. Armour, and A. Doufexi, *A distributed massive mimo testbed to assess real-world performance and feasibility*, in *Vehicular Technology Conference (VTC Spring), 2015 IEEE 81st*, pp. 1–2, IEEE, 2015.

[27] E. G. Larsson, O. Edfors, F. Tufvesson, and T. L. Marzetta, *Massive mimo for next generation wireless systems*, *IEEE Communications Magazine* **52** (2014), no. 2 186–195.

[28] J. Choi, D. J. Love, and P. Bidigare, *Downlink training techniques for fdd massive mimo systems: Open-loop and closed-loop training with memory*, *IEEE Journal of Selected Topics in Signal Processing* **8** (2014), no. 5 802–814.

[29] F. Rusek, D. Persson, B. K. Lau, E. G. Larsson, T. L. Marzetta, O. Edfors, and F. Tufvesson, *Scaling up mimo: Opportunities and challenges with very large arrays*, *IEEE Signal Processing Magazine* **30** (2013), no. 1 40–60.

[30] C. Shen and M. P. Fitz, *Mimo-ofdm beamforming for improved channel estimation*, *IEEE Journal on selected Areas in communications* **26** (2008), no. 6.

[31] U. Madhow, *Fundamentals of digital communication*. Cambridge University Press, 2008.

[32] A. Aragon-Zavala, *Antennas and propagation for wireless communication systems*. John Wiley & Sons, 2008.

[33] F. Quitin, A. T. Irish, and U. Madhow, *A scalable architecture for distributed receive beamforming: analysis and experimental demonstration*, *IEEE Transactions on Wireless Communications* **15** (2016), no. 3 2039–2053.

[34] S. Sesia, M. Baker, and I. Toufik, *LTE-the UMTS long term evolution: from theory to practice*. John Wiley & Sons, 2011.

[35] D. J. Love, R. W. Heath, and T. Strohmer, *Grassmannian beamforming for multiple-input multiple-output wireless systems*, *IEEE transactions on information theory* **49** (2003), no. 10 2735–2747.

[36] C. K. Au-Yeung and D. J. Love, *On the performance of random vector quantization limited feedback beamforming in a miso system*, *IEEE Transactions on Wireless Communications* **6** (2007), no. 2.

[37] N. Jindal, *Mimo broadcast channels with finite-rate feedback*, *IEEE Transactions on information theory* **52** (2006), no. 11 5045–5060.

[38] W. Shen, L. Dai, Y. Zhang, J. Li, and Z. Wang, *On the performance of channel statistics-based codebook for massive mimo channel feedback*, *IEEE Transactions on Vehicular Technology* (2017).

[39] J.-C. Shen, J. Zhang, K.-C. Chen, and K. B. Letaief, *High-dimensional csi acquisition in massive mimo: Sparsity-inspired approaches*, *IEEE Systems Journal* **11** (2017), no. 1 32–40.

[40] B. Lee, J. Choi, J.-Y. Seol, D. J. Love, and B. Shim, *Antenna grouping based feedback compression for fdd-based massive mimo systems*, *IEEE Transactions on Communications* **63** (2015), no. 9 3261–3274.

[41] H. Ji, Y. Kim, J. Lee, E. Onggosanusi, Y. Nam, J. Zhang, B. Lee, and B. Shim, *Overview of full-dimension mimo in lte-advanced pro*, *IEEE Communications Magazine* **55** (2017), no. 2 176–184.

[42] 3GPP, *Evolved Universal Terrestrial Radio Access (E-UTRA); Base Station (BS) radio transmission and reception*, TS 36.104, 3rd Generation Partnership Project (3GPP), Sept., 2008.

[43] I. Thibault, A. Faridi, G. E. Corazza, A. V. Coralli, and A. Lozano, *Design and analysis of deterministic distributed beamforming algorithms in the presence of noise*, *IEEE Transactions on Communications* **61** (2013), no. 4 1595–1607.

[44] P. Bidigare, M. Oyarzyn, D. Raeman, D. Chang, D. Cousins, R. O'Donnell, C. Obranovich, and D. Brown, *Implementation and demonstration of receiver-coordinated distributed transmit beamforming across an ad-hoc radio network*, in *Signals, Systems and Computers (ASILOMAR), 2012 Conference Record of the Forty Sixth Asilomar Conference on*, pp. 222–226, IEEE, 2012.

[45] S. Colieri, M. Ergen, A. Puri, and A. Bahai, *A study of channel estimation in ofdm systems*, in *Vehicular Technology Conference, 2002. Proceedings. VTC 2002-Fall. 2002 IEEE 56th*, vol. 2, pp. 894–898, IEEE, 2002.

[46] B. Mamandipoor, D. Ramasamy, and U. Madhow, *Newtonized orthogonal matching pursuit: Frequency estimation over the continuum*, *arXiv preprint arXiv:1509.01942* (2015).

[47] D. R. Brown III, U. Madhow, M. Ni, M. Rebholz, and P. Bidigare, *Distributed reception with hard decision exchanges*, *IEEE Transactions on Wireless Communications* **13** (2014), no. 6 3406–3418.

[48] J. Hu and N. C. Beaulieu, *Accurate simple closed-form approximations to rayleigh sum distributions and densities*, *IEEE Communications Letters* **9** (2005), no. 2 109–111.

[49] A. Wadhwa, U. Madhow, J. Hespanha, and B. M. Sadler, *Following an RF trail to its source*, in *Communication, Control, and Computing (Allerton), 2011 49th Annual Allerton Conference on*, pp. 580–587, IEEE, 2011.

[50] S. Venkateswaran, J. T. Isaacs, K. Fregene, R. Ratmansky, B. M. Sadler, J. P. Hespanha, and U. Madhow, *RF source-seeking by a micro aerial vehicle using rotation-based angle of arrival estimates*, in *American Control Conference (ACC), 2013*, pp. 2581–2587, IEEE, 2013.

[51] K. Becker, *Passive localization of frequency-agile radars from angle and frequency measurements*, *IEEE Transactions on Aerospace and Electronic Systems* **35** (1999), no. 4 1129–1144.

[52] N. H. Nguyen and K. Doğançay, *Single-platform passive emitter localization with bearing and doppler-shift measurements using pseudolinear estimation techniques*, *Signal Processing* **125** (2016) 336–348.

[53] A. Amar and A. J. Weiss, *Localization of narrowband radio emitters based on doppler frequency shifts*, *IEEE Transactions on Signal Processing* **56** (2008), no. 11 5500–5508.

[54] A. Tahat, G. Kaddoum, S. Yousefi, S. Valaee, and F. Gagnon, *A look at the recent wireless positioning techniques with a focus on algorithms for moving receivers*, *IEEE Access* **4** (2016) 6652–6680.

[55] H. Witzgall, B. Pinney, and M. Tinston, *Doppler geolocation with drifting carrier*, in *Military Communications Conference, 2011-MILCOM 2011*, pp. 193–198, IEEE, 2011.

[56] H. Witzgall, J. Covington, and A. Pierce, *Single aircraft passive doppler location of radios*, in *Aerospace Conference, 2015 IEEE*, pp. 1–8, IEEE, 2015.

[57] V. M. Baronkin, Y. V. Zakharov, and T. C. Tozer, *Cramer-rao lower bound for frequency estimation in multipath rayleigh fading channels*, in *Acoustics, Speech, and Signal Processing, 2001. Proceedings.(ICASSP'01). 2001 IEEE International Conference on*, vol. 4, pp. 2557–2560, IEEE, 2001.

[58] D. R. Brown III, Y. Liao, and N. Fox, *Low-complexity real-time single-tone phase and frequency estimation*, *IEEE Military Communication* (2010).

[59] M. Souden, S. Affes, J. Benesty, and R. Bahroun, *Robust doppler spread estimation in the presence of a residual carrier frequency offset*, *IEEE Transactions on Signal processing* **57** (2009), no. 10 4148–4153.

[60] B. Mamandipoor, D. Ramasamy, and U. Madhow, *Newtonized orthogonal matching pursuit: Frequency estimation over the continuum.*, *IEEE Trans. Signal Processing* **64** (2016), no. 19 5066–5081.

[61] I. Kaminer, A. Pascoal, E. Hallberg, and C. Silvestre, *Trajectory tracking for autonomous vehicles: An integrated approach to guidance and control*, *Journal of Guidance, Control, and Dynamics* **21** (1998), no. 1 29–38.

[62] D. R. Nelson, D. B. Barber, T. W. McLain, and R. W. Beard, *Vector field path following for miniature air vehicles*, *IEEE Transactions on Robotics* **23** (2007), no. 3 519–529.

[63] P. Sujit, S. Saripalli, and J. B. Sousa, *An evaluation of UAV path following algorithms*, in *Control Conference (ECC), 2013 European*, pp. 3332–3337, IEEE, 2013.